Summer 2023

Estimating Evapotranspiration and Analyzing Soil Moisture and Heat Flux Parameters at Taneum Creek, Central Washington

Edward Vlasenko
edwardv96@outlook.com

ESTIMATING EVAPOTRANSPIRATION AND ANALYZING SOIL MOISTURE AND HEAT FLUX

PARAMETERS AT TANEUM CREEK, CENTRAL WASHINGTON

_____

A Thesis

Presented to

The Graduate Faculty

Central Washington University

_____

In Partial Fulfillment

of the Requirements for the Degree

Master of Science

Geological Sciences

_____

by

Edward Vlasenko

August 2023

CENTRAL WASHINGTON UNIVERSITY

Graduate Studies

We hereby approve the thesis of

Edward Vlasenko

Candidate for the degree of Master of Science

APPROVED FOR THE GRADUATE FACULTY

_____   _____

                        Dr. Carey Gazis, Committee Chair

_____   _____

                        Dr. Lisa Ely

_____   _____

                        Dr. Clay Arango

_____   _____

                        Dean of Graduate Studies

ABSTRACT

ESTIMATING EVAPOTRANSPIRATION AND ANALYZING SOIL MOISTURE AND HEAT FLUX
PARAMETERS AT TANEUM CREEK, CENTRAL WASHINGTON

by

Edward Vlasenko

August 2023

In the past two decades, stream restoration work, primarily in the form of wood
emplacement, has been undertaken in the Taneum Creek watershed, resulting in increased
channel-floodplain connectivity. One of the goals of stream restoration was to boost dry season
groundwater storage in the shallow floodplain aquifer. However, any gains in groundwater due
to increased connectivity may be nullified by increased evapotranspiration (ET) losses because
of denser floodplain vegetation. Within the floodplain aquifer budget, ET is a major flow of
water out of the system and is not well quantified.

In order to quantify ET, a monitoring site was established to measure relevant
hydrological and environmental parameters along lower Taneum Creek in a meadow which
contains a new side channel and a series of beaver dams. The monitoring site includes an
evaporation station, and two soil monitoring locations, "riparian" and "meadow", representing
relatively wet and relatively dry areas within the Taneum floodplain respectively. This
monitoring equipment provided ground-truthing estimates of ET that were compared to
satellite-based estimates generated by OpenET.

Estimates of ET and evaporation using different methods were generated for a six week period in May to July, 2023. Two ET estimates were calculated using the Penman-Monteith FAO-56 method, using soil heat flux data collected in the field and local weather data. These two estimates, (1-7 mm/day at the riparian location and 0-6 mm/day in the meadow location), overlap significantly. These soil heat flux estimates increased as the season progressed, but were consistently lower than the satellite-based estimates, which range from 4-7 mm/day. This difference between estimates from different methods may be because the remote-sensing based estimates include transpiration from large trees that were not captured in the localized soil heat flux measurements. Evaporation calculated from pan evaporation, which excludes transpiration, displayed the lowest rate of water loss, at an average of 2 mm/day across the study period. Magnitude of ET fluxes suggests that any increase in inputs to groundwater storage [as a result of increased channel-floodplain connectivity] may well be negated by increased vegetation growth and associated evapotranspiration.

ACKNOWLEDGMENTS

TABLE OF CONTENTS

TABLE OF CONTENTS (CONTINUED)

Chapter   Page

LIST OF TABLES

LIST OF FIGURES

LIST OF FIGURES (CONTINUED)

x

CHAPTER I

INTRODUCTION

Evapotranspiration (ET) is the process by which water is transferred from the land surface and vegetation to the atmosphere through the combined processes of evaporation and transpiration. A notoriously difficult water budget component to quantify, ET plays a critical role in hydrologic cycling in both agricultural and natural settings. Quantifying evapotranspiration rates is important for managing water resources, especially in regions where water availability is limited. It is a major flux in all watersheds, and a necessary parameter for water budget calculations.

Understanding and calculating water budgets provides valuable insights into water availability, usage, and sustainability. Water budgets help to succinctly assess the net flows of water in a given area, allowing water managers to make informed decisions about water allocation, conservation measures, and sustainable use. Additionally, they are particularly helpful for managing groundwater resources, which by their nature are less-tangible than surface water resources and thus more difficult to monitor.

Governing Principles and Controlling Variables

Evaporation is the physical process by which water changes from a liquid to a gas and enters the atmosphere directly from the soil, water bodies, or other surfaces. Transpiration refers to the method by which plants release water vapor into the

atmosphere through their leaves. Evapotranspiration, the sum of these two components, is the total water loss from the planet's surface to the atmosphere. Because both evaporation and transpiration represent processes by which liquid surface water is converted to atmospheric water vapor, these functions are combined into the singular term, evapotranspiration (ET).

There are numerous factors which affect the rate of ET in a system. Affecting transpiration rates specifically are temperature, relative humidity, wind/air movement intensity, soil moisture availability, and the plant species, size, health, and growth rate. Increases in temperature, wind/air movement, and soil moisture availability are correlated with increased transpiration rate (Hanson, 1991; Rana & Katerji, 2000; Subedi & Chavez, 2015). Drier air (low relative humidity) near a plant is energetically favorable for increased transpiration, as this produces a greater concentration gradient between the leaf interior and surrounding air (Hanson, 1991). The factors influencing evaporation rate are similar. Affecting evaporation rates specifically are relative humidity, wind/air movement intensity, surface area, pressure, and temperature. Increased wind/air movement, surface area, and temperature are all correlated with a greater rate of evaporation. Similar to transpiration, a low relative humidity of the air (drier air) is associated with more intense evaporation (Hanson, 1991). Pressure plays a relatively minor role, but can be relevant in high elevation systems. Lower atmospheric pressure, such as at high elevations, reduces the energetic barrier water molecules must overcome to evaporate (Ohashi et al., 2020). Essentially, a lower pressure means there is less force to keep the molecules in a liquid state.

Quantifying ET

Effective estimation of ET water loss is essential for computing water balances and determining water availability. Historically, a wide variety of empirical and analytical methods have been developed and employed to measure ET, mainly in agricultural settings. Owing to its significance to agricultural production, research into ET within field settings is plentiful and provides a sound basis for quantifying ET. By possessing features and qualities such as relatively flat topography and uniform vegetation, agricultural settings provide a regularity and uniformity not present in a more "natural" setting such as a forest. Additionally, water inputs to the system are generally known, as these represent metered irrigation flows (Subedi & Chavez, 2015; Rana & Katerji, 2000).

ET in "natural" settings is considerably more difficult to measure, as these settings introduce numerous variables which complicate ET estimation. Local environmental factors such as spatial variability in soil profiles, vegetation, and topography influence the amount of water lost from a setting by ET, and make it more difficult to quantify.

One common and straight-forward approach is by soil-water balance. Soil-water balance is an indirect measurement method, and is best represented by the simplified equation:

$$P + I = ET \pm \Delta S \tag{1}$$

In Equation 1, P is precipitation, I is irrigation, ET is evapotranspiration, and ΔS is the change in soil moisture during the measurement interval. Generally, irrigation water supply is known, and precipitation is measurable through the use of rain gauges. For successful application of the equation, soil water content must be measured accurately and over a sufficient soil depth.

A similar approach is to employ surface-energy balance, which estimates ET by relating it to energy (heat) transfers between the surface and the atmosphere. A summary of all fluxes in surface energy balance can be seen below in Figure 1. This involves accurately measuring incoming and outgoing energy fluxes, including net radiation, sensible heat flux, latent heat flux, and ground heat flux. Surface energy balance is best summarized by Equation 2:

$$Rn = LE + H + G \tag{2}$$
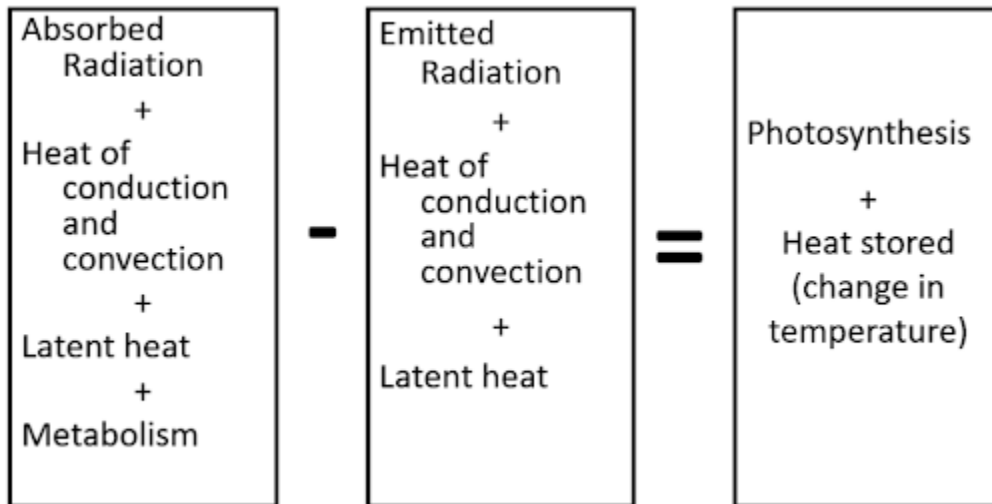
Figure 1. Visual diagram summarizing all surface energy balance fluxes. ET corresponds to absorbed latent heat, in the leftmost box. Emitted latent heat represents water vapor condensing into dew.

In Equation 2, LE refers to latent heat flux, H is the sensible heat flux, and G is the soil heat flux, and Rn is net radiation. Net radiation is defined as positive if heat is moving towards the surface (such as during the day, by sunlight), and negative otherwise. All other fluxes are defined as positive if heat is moving away from the surface. Sensible heat flux (H) refers to heat transfer between the ground and the atmosphere by conduction and convection. Soil heat flux (G) is the heat transfer between the surface and deeper soil, primarily by conduction. Within the surface energy balance model, evapotranspiration is represented by the latent heat flux. This is the thermal energy that is absorbed by water at the surface (in soil) as it undergoes a phase change from liquid to gas (evaporates). Mathematically, the latent heat flux is the product of the latent heat of vaporization of water, a constant, and the rate of evapotranspiration.

This study relies on the FAO-56 form of the Penman-Monteith equation to empirically calculate a daily "reference" ET for the Taneum field site. This calculated reference ET is meant to represent a hypothetical "average" crop at Taneum Creek, which contains a great diversity of vegetation types (Allen et al., 2005; Zotarelli et al., 2009). The Penman-Monteith equation represents a refined, widely used method for calculating reference evapotranspiration in mm/day based on the principles of surface energy balance. The equation combines various meteorological parameters to estimate daily actual evapotranspiration in a given setting. A summary of the equation and all input parameters can be seen in Equation 3 and Table 1 (Allen et al., 2005; Zotarelli et al., 2010).

$$ET_0 = (0.408 * \Delta * (R_n - G) + \gamma * (C_n / (T + 273)) * u_2 * (e_s - e_a)) / (\Delta + \gamma * (1 + C_d * u_2)) \quad (3)$$

Table 1. Summary of Penman-Monteith equation input parameters

Variable	Name	Units
ET_0	Reference evapotranspiration	mm / day
Δ	Slope of the saturation vapor pressure-temperature curve	kPa / ℃
R_n	Net radiation at the crop surface	MJ / m^2 / day
G	Soil heat flux density	MJ / m^2 / day
γ	Psychrometric constant	kPa / ℃
T	Mean daily air temperature at 2m height	℃
u_2	Mean daily wind speed at 2m height	m / s
e_s	Saturation vapor pressure	kPa
e_a	Actual vapor pressure	kPa
C_n	Numerator constant for reference crop type	
C_d	Denominator constant for reference crop type	

Remote Sensing

In recent years, remote-sensing based approaches have become the new gold standard for measuring ET (Kalma et al., 2008; McCabe et al., 2019). Remote sensing-based methods for measuring ET use satellite images to estimate the amount of water that is being lost from the land surface. These methods are based on the principle that vegetation absorbs and reflects different wavelengths of radiation (light), and that the

6

amount of absorbed and reflected light is a measure of energy that is related to the amount of water that is being lost through transpiration.

The advantage of remote sensing-based methods for measuring ET is that they can cover large areas and provide spatially explicit estimates of evapotranspiration rates. They are also non-invasive and can be used in areas that are difficult to access, such as remote, protected, or mountainous regions. Another advantage is that remote sensing-based methods can be used to monitor evapotranspiration rates over time, allowing for changes in water consumption to be identified and managed.

However, remote sensing-based methods also have some disadvantages. They rely on the availability of satellite data and meteorological data, which may not always be available at the desired spatial or temporal resolution. The accuracy of remote sensing-based estimates can also be affected by cloud cover, atmospheric conditions, and the complexity of the land surface being monitored.

Yakima Basin – Climate and Hydrology

The headwater tributaries of the Yakima River flow down the eastern slopes of the Cascade Mountains, providing essential freshwater resources to residents of central Washington and a $4 billion agricultural industry during the dry summer months (Meseck, 2020). A map of modern Yakima Basin land cover, demonstrating the dominance of the agricultural industry in the region and providing context for this study can be seen in Figure 2.
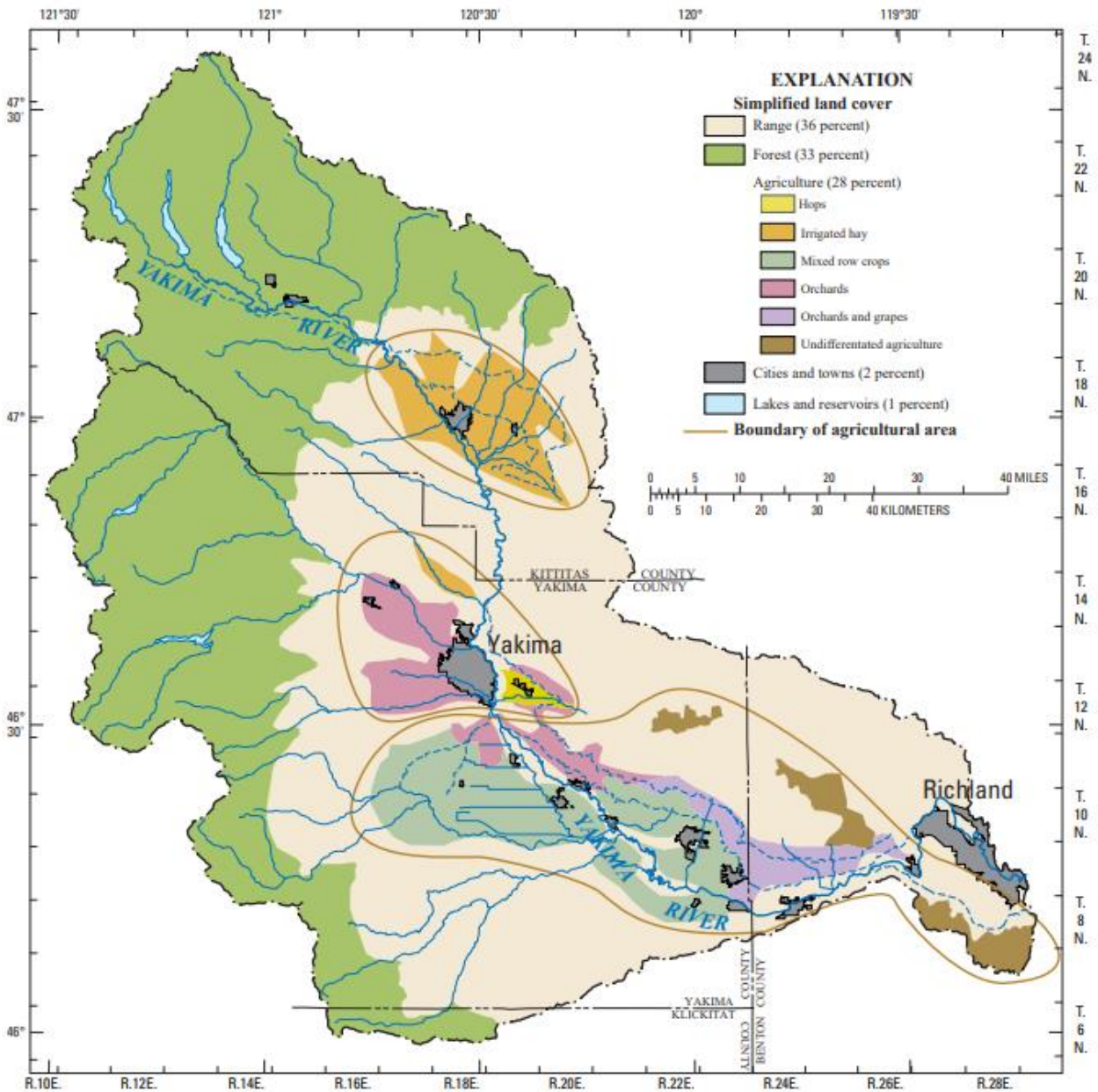
Figure 2. This map visualizes the major crops produced by the basin's agricultural industry. The legend indicates that agricultural land alone constitutes 28% of the Yakima watershed's total land area. An additional 36% percent of land is used for cattle ranging, which is greater than the 33% of land that still remains as forest.

The Yakima River Basin experiences a "Mediterranean"-type climate, characterized by hot, dry summers and cold, wet winters. The region receives most of its precipitation during the winter months, primarily in the form of snowfall in the higher elevations (Figure 3). The snowpack serves as a critical natural reservoir, storing water during the winter and releasing it gradually during the spring and summer as temperatures rise and snow melts.

Spring snowmelt is a crucial component of the hydrologic regime in the Yakima River Basin. The melting snow contributes to streamflow and replenishes the water supply for irrigation, municipal, and environmental needs. The timing and rate of snowmelt play a significant role in determining water availability and streamflow throughout the year.

The snowpack of the Cascade mountains, upon which the various users of the basin rely, is forecasted to decrease in response to the changing climate. Earlier and reduced snowmelts, earlier onset of summer droughts, and increased drought frequency are all anticipated changes to the basin's hydrological regime (Vano et al., 2010; Gergel et al., 2017; Malek et al., 2010).
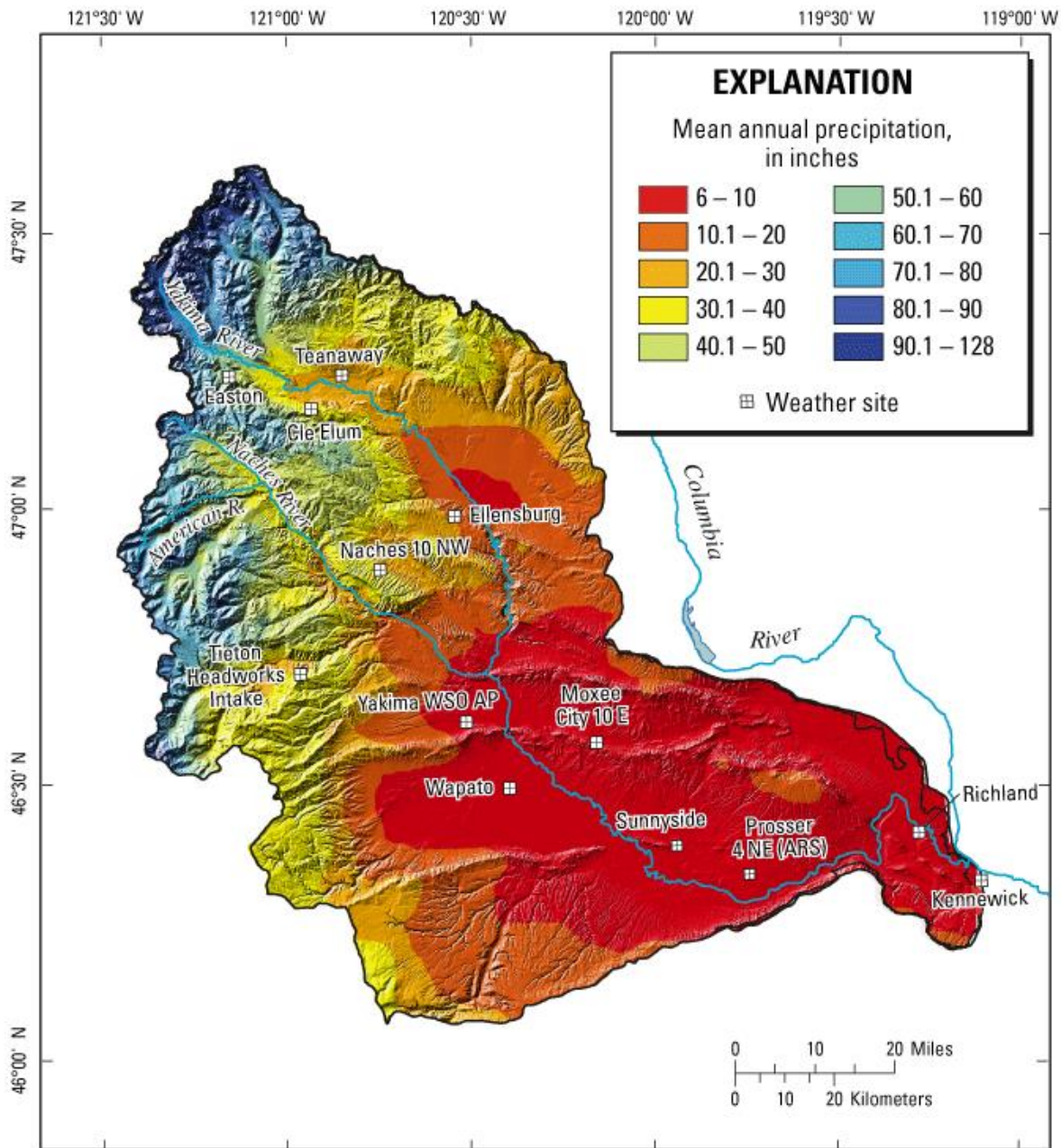
Figure 3. Most of the watershed's precipitation occurs in the highlands to the north and west. The west-east precipitation gradient is facilitated by the region's topography. The Cascade Mountains in the west lead into the Yakima Fold and Thrust belt, and from there to the mouth of the Yakima River in Kennewick. The agricultural areas defined in Figure 2 correspond to the areas of lowest precipitation within the region. Water demand is greatest where its availability is least.

Yakima Basin – Timber Logging and Stream Restoration

The upper Yakima River Basin was heavily exploited by the timber industry during the early 20th century (Henderson, 1990; Collins et al., 2016). Tributary river systems such as Taneum and Teanaway functioned as a pipeline for timber transportation downstream through the destructive practice of splash damming. This immensely erosive practice stripped streams of their natural large wood and sediment accumulations, resulting in rapid incision into the bedrock below at many locations. In an effort to restore these river systems to a more natural state and restore habitat for wildlife, especially native fish species, numerous large wood restoration projects were conducted at tributaries throughout the upper basin (Collins et al., 2016).

The primary goals of these wood-based restoration projects are to provide fish habitat, reduce bank erosion and re-aggrade channel bed sediment, and increase channel-floodplain connectivity (Roni et al., 2015; Collins et al., 2012). Research suggests that large wood facilitates groundwater connectivity by diverting water from the main channel onto the floodplain during high flows, promoting increased infiltration into the subsurface (Collins et al., 2012). This groundwater connectivity is essential for supporting the life cycles of fish and other aquatic organisms (U.S. Bureau of Reclamation and WA Department of Ecology, 2012).

Yakima Basin - Water Budget

Vaccaro et al. (2009) of the USGS developed a hydrogeologic framework for the Yakima River Basin groundwater system, including water budgets for modern and pre-development conditions (Table 2). In both scenarios, ET represents the most significant flux in the system. A majority of the basin's water is consumed each year by ET, emphasizing the importance of quantifying and understanding ET values for effective management.

Table 2. Yakima River Basin Water Budget (from Vaccaro et al., 2009)

Water Budget Component	Predevelopment	Modern
Precipitation	8.6	8.6
Streamflow	4.1	2.5
Evapotranspiration	5.1	6.1
Recharge*	3.8	5
Pumpage	0	0.24
Reservoir Storage	0	1.1
Diversions**	0	3.1

Summary of water budget data for the Yakima River Basin for predevelopment (no white settler activity) and modern conditions. All values are in millions of acre-ft. Irrigation agriculture and other elements of European civilization have resulted in significantly decreased streamflows and increased recharge and ET, when compared to "natural" conditions.

Yakima Basin - Water Management

Water management in the Yakima River Basin is complex and involves a system of reservoirs, diversions, canals, and pipelines. These infrastructure elements are designed to capture and store water during periods of high flow, such as during snowmelt or periods of heavy rainfall, and release it during times of lower natural flow,

typically during the dry summer months. The storage and regulated release of water from reservoirs help meet various water demands, including irrigation for agricultural purposes, municipal water supply, hydropower generation, and supporting fish habitat.

In the early 2000s, a diverse set of stakeholders in central Washington came together to develop a comprehensive plan to tackle the collection of hydrological issues facing the Yakima River Basin. This collaboration came to be known as the Yakima Basin Integrated Plan (YBIP), a comprehensive 30-year water management plan that aims to balance a myriad of private, local, tribal, state, federal, and environmental interests. Some example partners include the US Bureau of Reclamation, Yakama Nation, WA Dept. of Ecology, and various local irrigation districts (YBIP, 2023).

The plan is significant because it provides a collaborative, science-based approach to address water management challenges in the basin, which has faced conflicts over water use and declining fish populations for decades. The development of the YBIP is meant to address current and future water issues by focusing on seven key elements: "reservoir fish passage, structural and operational changes, surface water storage, groundwater storage, habitat/watershed protection, enhanced water conservation, and market reallocation" (Figure 4). Each plan element plays an important role in ensuring a sustainable and productive future for all Yakima River Basin residents. More than 70 projects extend across the region from headwater streams in the upper basin to the river mouth in the Tri-Cities, where the Yakima drains into the Columbia (YBIP, 2023).

The funding for the YBIP comes from a combination of federal, state, and local sources. The federal government has provided funding through the Bureau of Reclamation's WaterSMART program, as well as through appropriations from Congress. Finally, local stakeholders have contributed funding through assessments and other means (YBIP, 2023).

This study falls under the groundwater storage component of the YBIP, which aims to find new opportunities for water storage. Previously mentioned large wood restoration efforts may facilitate natural floodplain water storage by diverting and slowing flows during the spring snowmelt. Increased floodplain aquifer storage during summer months would improve flow regimes and lower instream water temperatures, benefitting aquatic fauna (U.S. Bureau of Reclamation and WA Department of Ecology, 2012). However, any benefits in floodplain groundwater storage may be counteracted by increased vegetation growth and the resultant increase in evapotranspiration. This study aims to provide lower and upper bound estimates of evapotranspiration, a largely unknown water budget component, for lower Taneum Creek.
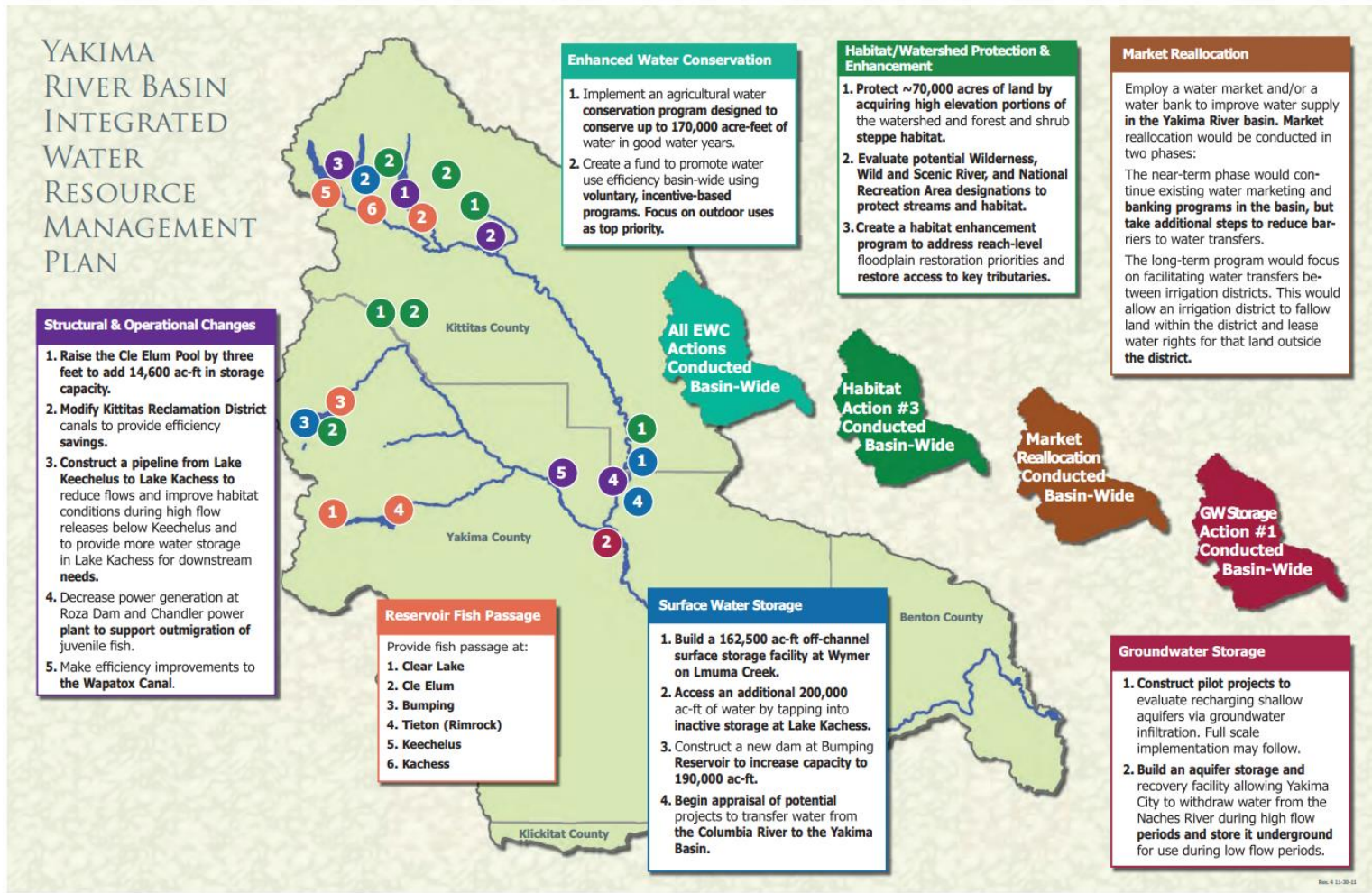
Figure 4. The seven elements of the Yakima Basin Integrated Plan. This study is a part of the groundwater storage and habitat/watershed protection & enhancement elements (WA Dept. of Ecology).

CHAPTER II

STUDY SITE BACKGROUND

Taneum Creek is located within Kittitas County in central Washington, approximately 17km northwest of Ellensburg. The stream flows from west to east and joins the Yakima River at mile 166.1 (Monk, 2009). The total area of the Taneum Creek basin is approximately 215 sq km (Jones & Stokes, 1991). Elevation ranges from about 1914m near Quartz Mountain to 515m at the Yakima River confluence (Toth, 1995; Jones & Stokes, 1991). Annual precipitation ranges from >150 cm in the upper Taneum to approximately 25 cm near the Yakima River confluence (Jones & Stokes, 1991).

Land Use History

The Yakima River Basin was used by local indigenous groups for hunting, fishing, and gathering. It is the historic home of the Yakama people, for which the greater river basin is named. Today, many of the Yakama people reside on a reservation in the lower basin. The Yakama Nation plays an active role in fisheries and water management within the basin.

European settlers began to arrive in great numbers to central Washington (then part of the Oregon territory) in the latter half of the 19th century. Logging activities began in the early 20th century, with many old-growth forests being cleared for timber. At this time, harvested logs were collected en masse in ponds created by the damming

of a local stream. When harvest in the area was complete, the dam holding the log-filled

pond would be blown with dynamite. The resulting cascade of floodwaters would float

the wood downstream where it would then be collected. This destructive practice had a

significant impact on the ecosystem, altering the composition of the forest and

disrupting the natural flow of water in the area (Figure 5). It resulted in immense erosion

of alluvial sediments, incising some areas of some streams all the way to bedrock

(Henderson, 1990; Abbe & Montgomery, 1996).
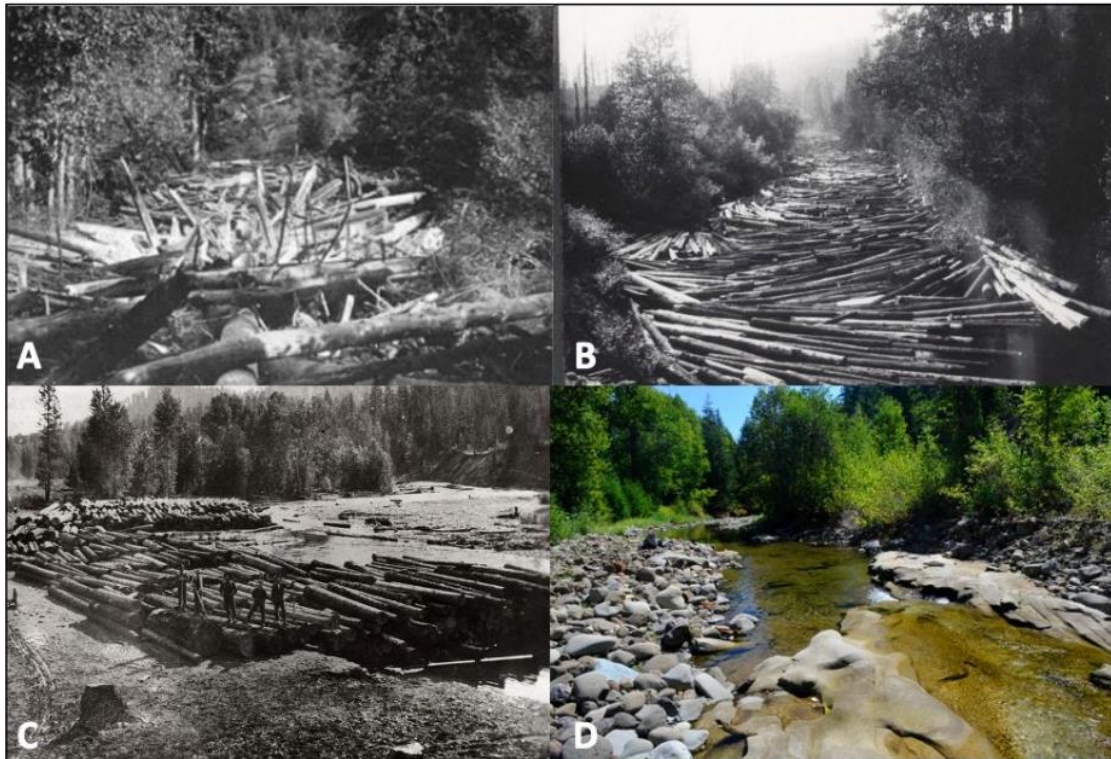
Figure 5. Figure adapted from Polizzi (2023) showing historical logging at the Teanaway River, another local tributary of the Yakima River. These activities were also conducted in the Taneum Creek watershed (Henderson, 1990). Photographs show conditions prior to, and after disruptive logging practices. A. Natural "log jam" in the Teanaway watershed prior to widespread onset of logging (Russell, 2016). B. Teanaway log drive: logs were collected in a pond behind a dam, before being sent downstream to a processing mill via controlled dam explosions (Henderson, 1990). C. Decking logs on the Teanaway River: logs would be loaded into the river behind a temporary dam structure The Frederick Kruger Collection, 1920). D. Modern day scoured bedrock appearance of the Teanaway River channel (Schanz et al., 2009).

In the mid-20th century, mining operations for precious metals were also established in the region, further altering the landscape and introducing new environmental risks. Logging and mining activities continued for several decades, declining over the 1930s and 1940s. Industrial activity within the Taneum valley included establishment of a railroad line, by which harvested goods were exported. This railroad line, which served to even further channelize the river, was removed in 1954. While logging and mining activities in the Taneum Creek watershed have declined significantly, some logging operations still occur in the region, albeit on a smaller scale. In addition, there are also some active mining claims in the area, though any mining activity is negligible (Henderson, 1990).

Today, Taneum Creek is used primarily for recreation. The area is popular among outdoor enthusiasts for activities such as hiking, hunting, fishing, and motorbiking. It also plays a critical role in fish ecology, providing habitat for young trout and salmonid fry.

In recent years, the Taneum Creek watershed has been the subject of extensive restoration work. These efforts have included the removal of a small dam, irrigation screening diversions, building fish passages, and the addition of large woody debris to the channel and floodplain. A map that delineates the watershed boundaries and labels locations of large wood additions can be found in Figure 6. Constructed in the late 1980s and early 1990s, the fish passageway opened up upper reaches of the stream for spawning fish (Monk, 2015).
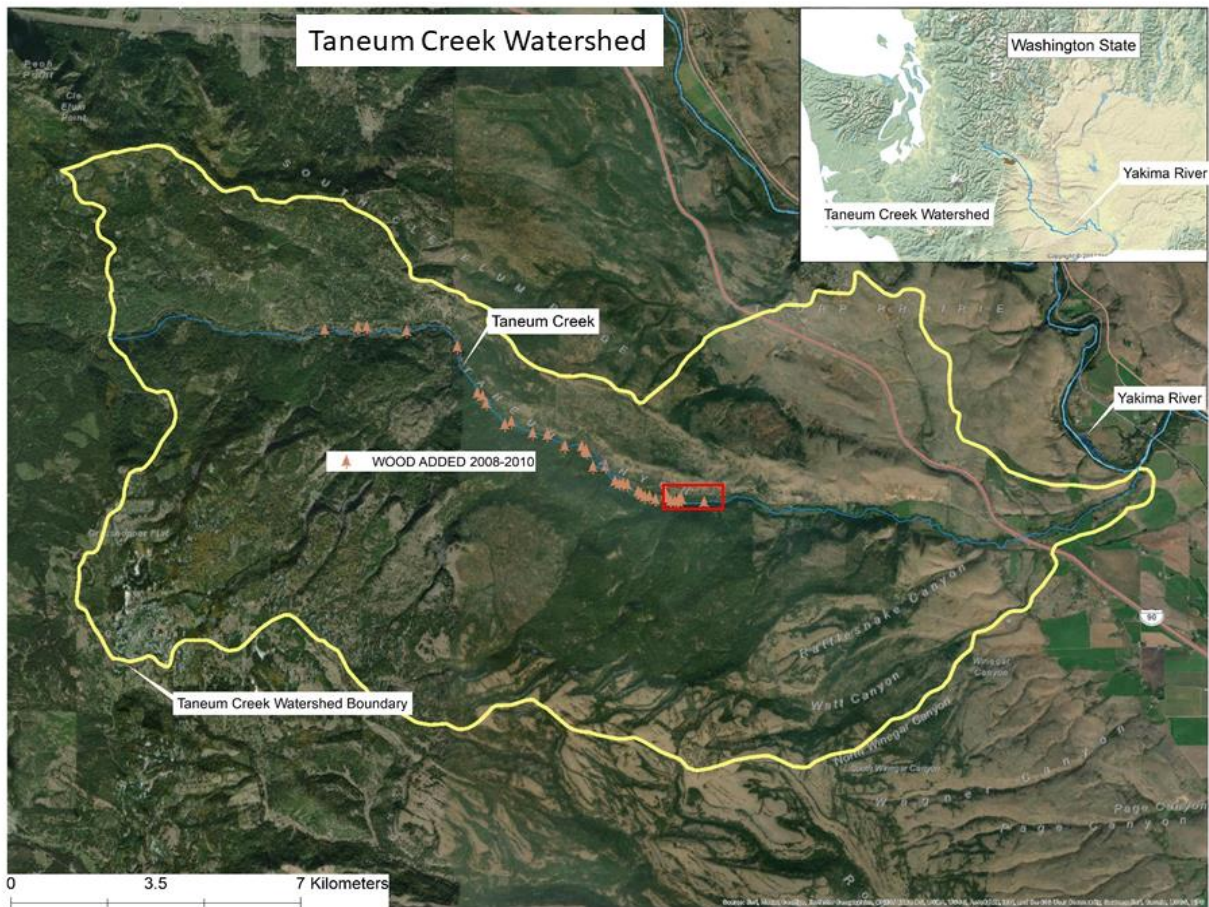
Figure 6. This image displays the Taneum Creek watershed. The lower watershed boundary of Taneum Creek and the creek itself are highlighted, along with the proximity to the Yakima River. The inset map in the top right corner displays the location of the Taneum Creek watershed and the Yakima River within the broader context of Washington state. Large woody debris addition sites are mapped for the 2008-2010 stream restoration projects (Ely & Gazis, 2021)

Several graduate students from Central Washington University have continued

research into the geomorphology, stratigraphy, and hydrology of Taneum Creek. Fixler

(2022) studied channel response to restoration via additions of large wood. His results

suggest that large woody debris plays a pivotal role in facilitating geomorphologic

channel change during flood events. During floods, individual logs mobilize and tangle

19

with each other, congregating into large log jams that can trap sediment and alter streamflow. Of the side channels that formed in stream reaches containing large wood, greater than 50% formed less than 10m downstream of a log jam (Fixler, 2022). Additionally, reaches of Taneum Creek with greater channel complexity displayed increased floodplain greenness and connectivity, suggesting increased water consumption and evapotranspiration (Fixler, 2022). Fixler's research suggests that large wood functions as a significant agent of hydrologic and geomorphic change at Taneum Creek.

More recently, Emily Polizzi examined the floodplain stratigraphy at Taneum in an effort to quantify the potential floodplain aquifer capacity. Through a combination of field work, mapping, and grain-size analysis, Polizzi estimated the floodplain area of Taneum to be 587-693 acres, and the capacity of the floodplain aquifer at 352-1,320 acre-ft (Polizzi, 2023).

Overall, the land use history at Taneum Creek reflects a complex interplay between human activities and the natural environment. While some of these activities have had negative impacts on the ecosystem, others have helped to preserve the region's natural beauty and provide opportunities for outdoor recreation.

Geology of Taneum Creek

A map of surface geology in the Taneum canyon can be found in Figure 7. The lower Taneum Creek study area is underlain by flows in the Grande Ronde member of the Columbia River Basalt Group. Surface deposits across the width of the valley

consist of unconsolidated or semi-consolidated alluvial clay, silt, sand, gravel, and cobbles. Within the valley, peat, artificial fill, and marsh, landslide, lahar, glacial, colluvial, volcaniclastic, and tephra deposits are also present (Lewellen et al., 1985).

Southern and northern valley walls consist mostly of Miocene fine-grained flood basalt flows (Lewellen et al., 1985). Valley walls also consist of flood basalt sills and dikes, hyaloclastite, pillowed lava flows, and peperites (Lewellen et al., 1985). Intercanyon areas consist of, saprolites, and pillow-palagonite complexes (Lewellen et al., 1985). Plagioclase-phyric flood basalt in the canyon is commonly interbedded with tuffaceous sandstone, siltstone, and conglomerate, most of which are parts of the Ellensburg and Latah Formations (Lewellen et al., 1985). Southern and northern valley slopes contain mostly landslide deposits, talus, colluvium, protalus ramparts, and 1980 ash from Mount St. Helens (Lewellen et al., 1985).
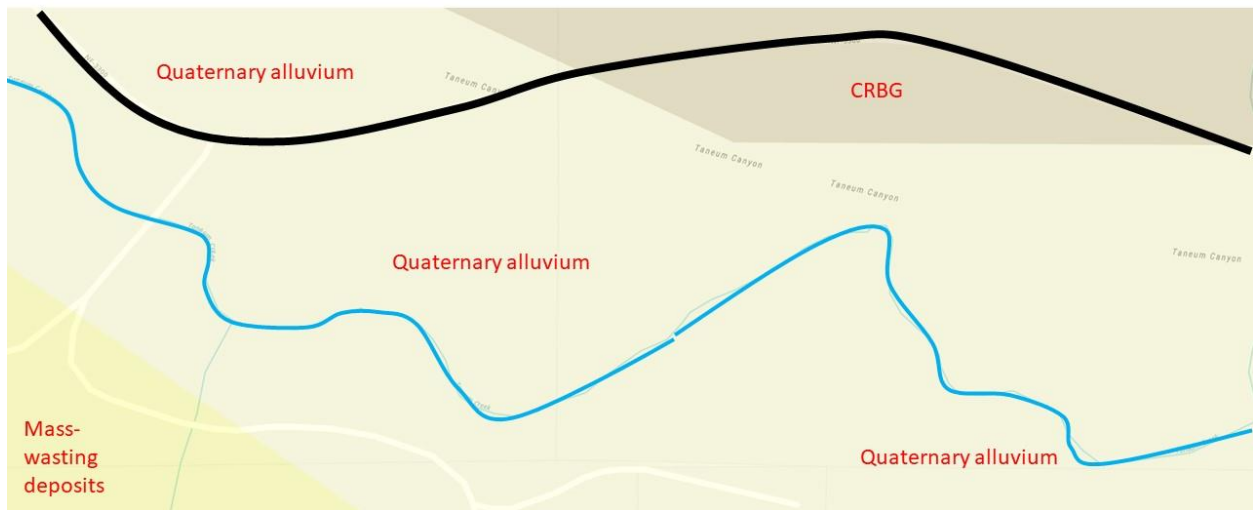
Figure 7. Summary map of surface geology at the Taneum study site. The West Taneum Road is outlined in black. The thinner blue line represents the main channel of Taneum Creek. Surface geology within the Taneum canyon consists primarily of Quaternary alluvium on the valley floor. Basalts of the Columbia River Basalt Group (CRBG) compose the northern ridge of the watershed.

21

Hydrogeology of Taneum Creek

The Taneum Creek watershed is underlain by two distinct hydrogeologic bedrock units: basalts of the Columbia River Basalt Group (CRBG) and older bedrock which lies beneath the CRBG flows in the study area and is exposed in the upper reaches of the Taneum watershed (Vaccaro et al., 2009).

In the upper reaches of the Taneum watershed, groundwater moves through fracture systems within Paleozoic metamorphic rocks (Ely et al., 2011; Gendaszek et al., 2014). In contrast, the lower portion of the basin is dominated by the groundwater regime of the CRBG rocks (Vacarro et al., 2009). Together, these geologic structures combine to form the aquifer system of the Taneum basin.

The alluvial floodplain aquifer examined in this study is maintained by these units and/or sedimentary layers such as the Ellensburg Formation (Vaccaro et al., 2009).

At Taneum Creek, groundwater and surface water interact, providing a variety of environments for the resident fauna, especially fish. Taneum Creek's flows are maintained by a combination of groundwater and surface water recharge. During the summer dry season, the creek's discharge is driven primarily by groundwater baseflow (Monk, 2009). Characterizing and understanding groundwater-surface water interactions is essential for environmental and agricultural uses.

100-yr Flood of 2011

On May 15th, 2011, Taneum experienced a large flood event during the spring snowmelt. Using a rating curve and flow measurements taken during the event, the discharge of this flood was estimated by Tappel (2012) to be 69 -79 m^3/s (2,400 to 2,800 cfs). As noted in the report, Tappel (2012) stated that though his measurements "were done without the stringent standards employed by the USGS, the confidence in the discharge range was high. The discharge estimate was approximately 11 - 23 m^3/s [400-800 cfs] above the 100-year flood threshold of 57m^3/s [2,000 cfs]" (Tappel, 2012). Most of the logs placed by the Yakama Nation in the years prior were mobilized and became tangled, creating large jams of woody debris and sediment (Tappel, 2012). However, emplaced logs did not travel downstream so far as to impact landowners (Tappel, 2012). Photographs taken of the flood event by Paul Tappel can be found in Figures 8 and 9.

Figure 8. This photograph was taken during the large flood of May 5th, 2011 near the intake to the Taneum irrigation canal at the downstream end of the watershed. Photo taken by Paul Tappel, 2011.

Figure 9. Another view of the Taneum Creek flood of May 5th, 2011. Photo taken near the intake to the Taneum irrigation canal by Paul Tappel, 2011.

CHAPTER III

METHODS

This study employed extended monitoring of numerous environmental and hydrological parameters in order to estimate and calculate for evapotranspiration. All environmental data was collected on a 15-minute time interval. Daily totals (soil heat flux) and daily averages (all other ET calculation input parameters) of values were derived from this 15-minute interval time series data.

Aerial Photography

A Ricoh GR II camera installed in a SmartPlanes Freya model drone was used to collect aerial imagery of the study site. Flights were conducted on May 2nd, May 26th, June 7th, and June 29th, 2023.The flight plan used in the aerial photography can be seen below in Figure 10. Each flight would generate between 200-400 photos, which were then stitched together into a single orthomosaic using the Agisoft Digital Pro software.
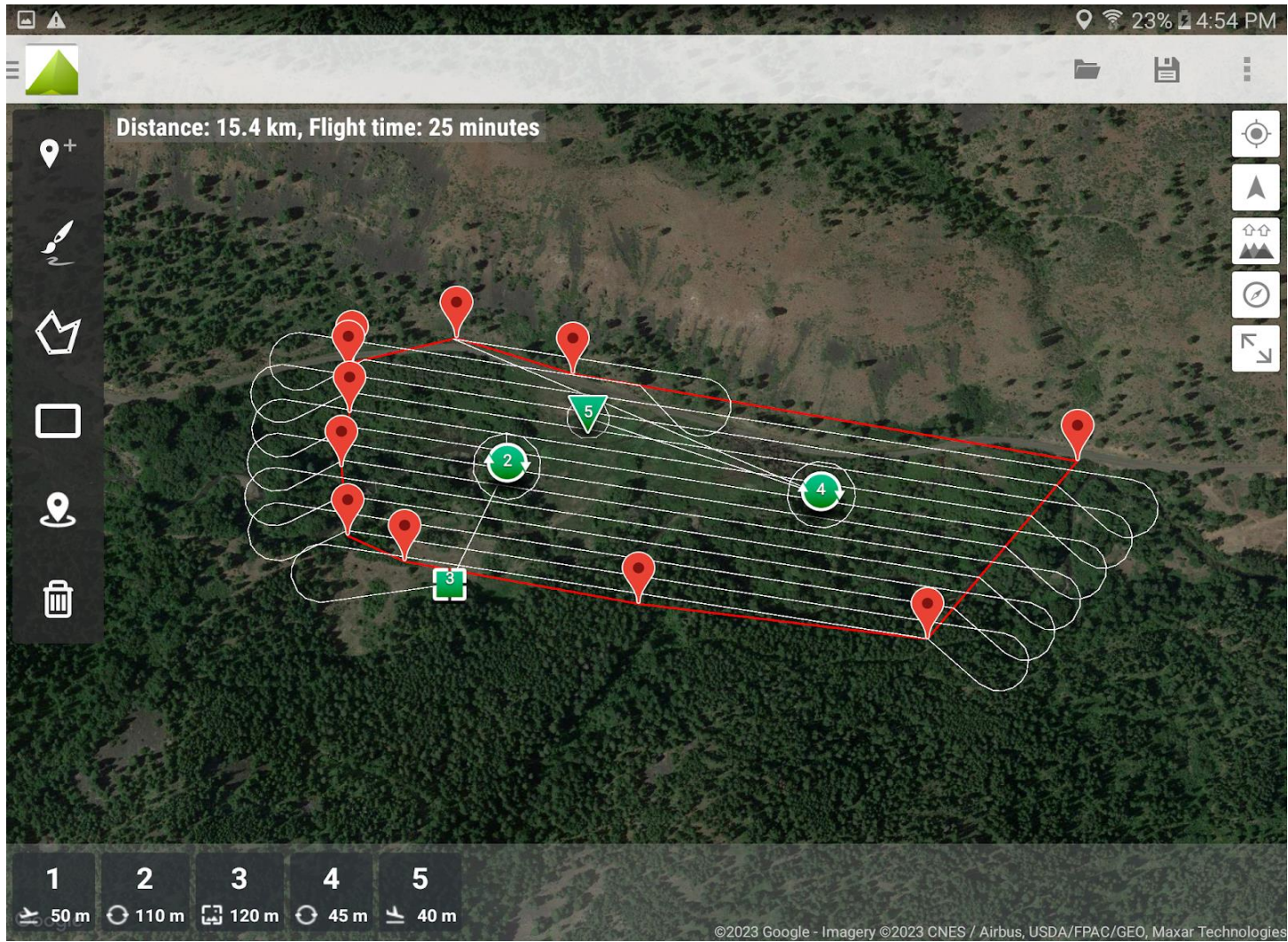
Figure 10. This figure shows the drone's flight path overlain on Google Earth imagery of the Taneum field site. The flight plan used in this study is identical to the path employed by Fixler (2022) in his aerial photography of the Taneum "Lower Reach".

27

Environmental Monitoring

Evaporation station:

An evaporation station consisting of a NovaLynx 255-200 Class-A evaporation pan with a 255-100 evaporation gauge and 255-704-B datalogger was deployed in the Taneum meadow to estimate evaporation. The ground surface was leveled, and the evaporation station was set up on top of a platform consisting of two standard 121.9 x 101.6 cm (48 in x 40 in) wooden pallets. The pan was filled with water, and exposed to the elements to represent evaporation from an open body of water (Figure 11).

During each site visit, evaporation data was downloaded from the datalogger. A manual measurement of pan water level was also taken and compared to the datalogger value. These manual measurements were always within 1cm of the water level indicated on the datalogger. In order for the evaporation pan to measure accurately, the water level in the pan must be kept between 12.7 and 22.9 cm (5 to 9 in). If the water level was becoming low, the pan would be replenished with water from the nearby Taneum Creek main channel. The volume of water used to replenish the plan was recorded.

Precipitation gauge:

Precipitation at Taneum Creek was measured directly with a precipitation gauge set up next to the evaporation station (Figure 11). Precipitation was measured and recorded at the time of each field site visit, and then the gauge would be emptied.

Figure 11. Photograph of evaporation station next to soil monitoring "riparian" site. The station is surrounded by 4 ft tall chicken wire fencing to discourage larger animals from drinking from the pan. The tall white cylinder is the evaporation gauge, which is directly connected to the pan and records its water level. A precipitation gauge seen next to the pan (transparent) was also deployed here.

Soil heat flux plates:

Two HFP01 Huskeflux heat flux plates were used to quantify soil heat flux in the Taneum meadow. Both plates were wired to their own CR23X dataloggers. The flux plates were buried at two different sites, representing "wet extreme" and "dry extreme" areas (Figures 12 and 13). Each plate was installed at the standard 5.0cm depth.

Soil moisture probes:

Four S-SMC-M005 EC5 Soil Moisture Smart Sensors were wired to HOBO dataloggers. Similar to the soil heat flux plates, the sensors were buried at two different sites, representing "wet extreme" and "dry extreme" areas (Figures 12 and 13). Sensors were installed at 2in, 4in, 6in, and 8in depth.

Thermocouples:

Two thermocouples were wired to each CR23X datalogger to track soil temperature. One thermocouple was installed at 10.0cm depth, and the other at 5.0cm depth.

Net radiometer:

A Delta-T Devices NR2 dome net radiometer was connected to a CR23X datalogger, and deployed along with the other environmental monitoring equipment in the relatively dry Taneum meadow. The net radiometer was connected to a 160 cm (3 ft) pipe, and attached to a ladder, in order to suspend the device above the height of the

tall grass, and away from any shadows. Tent stakes were tied to the ladder with rope to

secure the ladder-radiometer setup in the frequent high wind conditions present at the

field site.
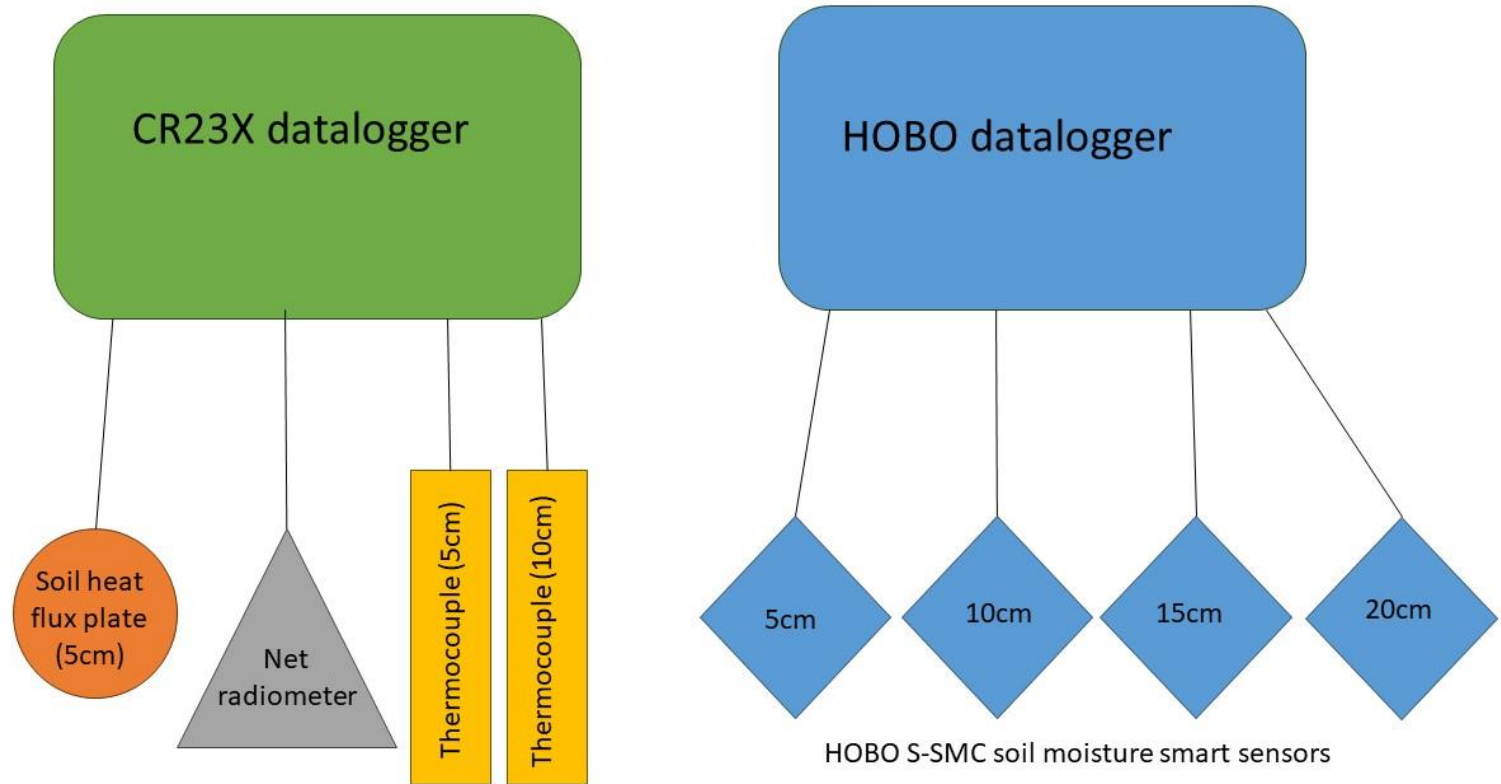
Figure 12. Summary of all environmental monitoring equipment deployed at the (relatively dry) meadow soil monitoring location. All sensors but the net radiometer were buried in the floodplain soil, with their burial depths labeled in the diagram. Connecting lines represent wired connections. The net radiometer was suspended above the meadow grass by use of a standing ladder.
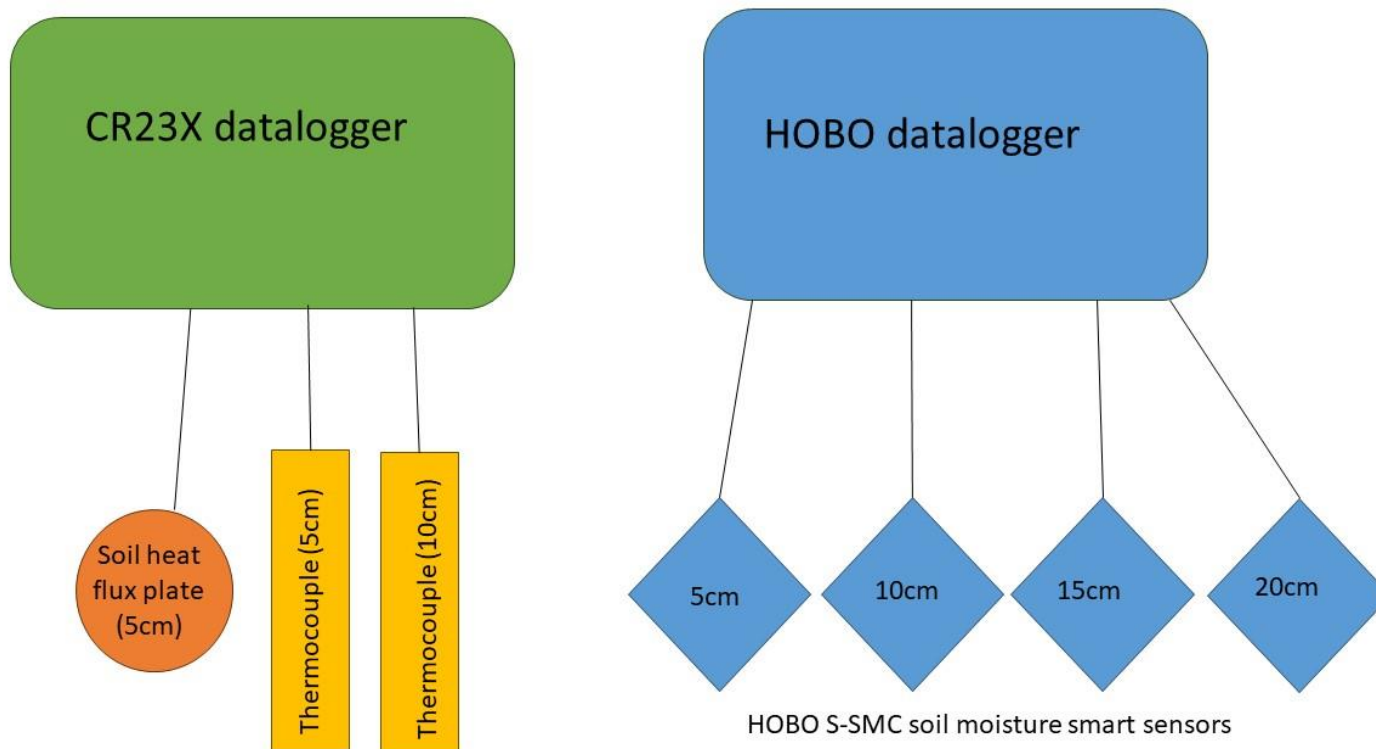
Figure 13. A concise visual summary of all environmental monitoring equipment deployed at the (relatively wet) riparian soil monitoring location found near the Taneum main channel. All sensors were buried in the floodplain soil, with their burial depths labeled in the diagram. Connecting lines represent wired connections. In addition to this equipment, the evaporation station was also deployed at this site.
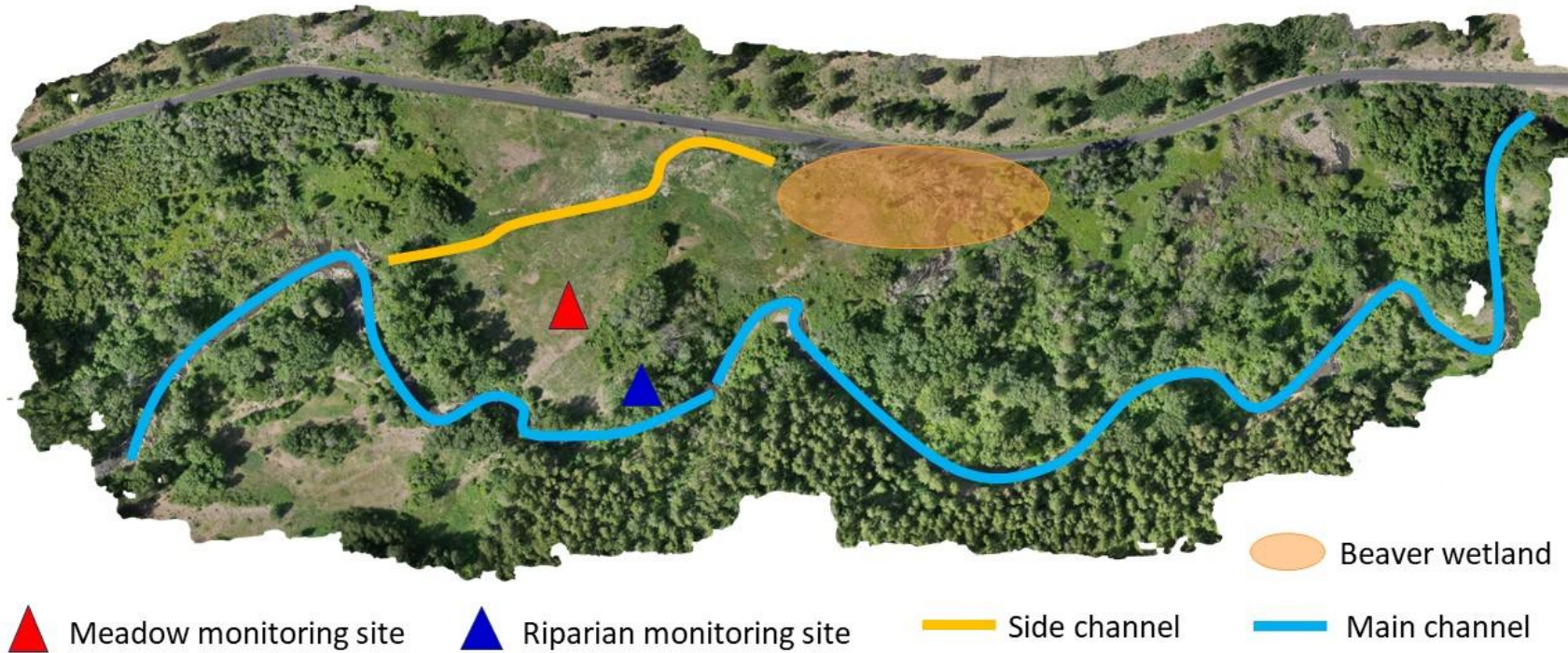
Figure 14. Visual overview of the location of deployed environmental monitoring equipment. The top of the imagery is bounded by West Taneum Rd and a steep ridge. Labeled with colored triangles, the two environmental monitoring sites were established on the floodplain between the main and side channel of Taneum Creek. The main and side channels are outlined in blue and yellow, to increase visibility. The side channel feeds a beaver wetland area (orange oval), which then drains back into the main channel of Taneum at several vegetation obscured points towards the right side of the composite image. The riparian monitoring location includes the evaporation station as well as soil probes.

Pan Evaporation Correction

An evaporation pan is a common and straightforward method for estimating ET in the field. Due to the nature of the pan model, pan evaporation often represents an overestimation of actual evaporation. A pan coefficient is used to convert pan evaporation rates to corresponding corrected evaporation rates. In this study, the pan coefficient was calculated by the FAO-56 method (Allen et al., 1998) using Equation 4. Pan coefficients were calculated using weather data from a WSU AgWeatherNet station in Thorp, WA, and ranged from 0.48 to 0.71 (AgWeatherNet, 2023).

$$Kp = 0.108 - 0.0286 * u2 + 0.0422* \ln(F) + 0.1434* \ln(H) - 0.000631* [\ln(F)]^2 * \ln(H) \quad (4)$$

Table 3. Summary of Pan Coefficient Equation Variables

Variable	Name	Units
u2	Wind speed at 2m height	m/s
F	Fetch distance	m
H	Mean relative humidity	%

Calculation of ET Using the Penman-Monteith Method

Reference ET for lower Taneum was calculated using the FAO-56 version of the Penman-Monteith equation shown in Equation 3 (Allen et al., 1998; Zotarelli et al., 2010). Weather data was sourced from Washington State University's AgWeatherNet (AWN), specifically the Thorp weather station (AgWeatherNet, 2023). For this study, 15

minute data was downloaded and used to calculate daily averages of relevant weather parameters such as wind speed, air temperature, and relative humidity.

This study relies on the Penman-Monteith equation to empirically calculate reference ET for the Taneum field site. The Penman-Monteith equation represents a refined, widely used method for calculating reference evapotranspiration in mm/day based on the principles of surface energy balance. The equation combines various meteorological parameters to estimate daily actual evapotranspiration in a given setting. A summary of the equation and all input parameters can be found in Equation 3 and Table 1.

In this study, 1250 was used as the numerator constant, and 0.36 as the denominator constant. These values are the arithmetic means of the short and tall reference crop constants (Allen et al., 2005; Zotarelli et al., 2009), representing a hypothetical "intermediate" reference crop constant which better represents the mixed vegetation present at Taneum. A sensitivity test of the numerator and denominator constants was conducted, but the difference between ET calculated by tall versus short crop constants was 5% or less for all but one of the study days. On this day, June 12th, there was an anomalously high soil heat flux total at the riparian monitoring site, producing the discrepancy.

CHAPTER IV

RESULTS AND DISCUSSION

Qualitative Aerial Imagery Analysis

Analysis of aerial photos is useful for quickly identifying trends in vegetation and water level. Composite aerial photos of the study site for the dates of May 2nd, May 26th, June 7th, and June 29th, 2023 can be found in Appendix C. In the aerial imagery, the main channel of Taneum Creek can be seen meandering, flowing west to east (left to right in the composite images). At the first sharp bend, some of the stream's discharge cuts through the channel walls, escaping and flowing out onto the floodplain. This forms a side channel which feeds into a downstream beaver wetland, where water seems to slow down and pool. Numerous fallen logs and dam structures can be seen in this beaver wetland area. On the north side, the wetland is bounded by the road. The beavers seemed to have cleverly used the road as one of the retaining walls for their flooded wetland area. The wetland drains back into the main channel of Taneum Creek at several different vegetation-obscured outlets found at the right side of the drone imagery. The number of drainage outlets at any given time seems to be dependent on the side channel discharge intensity (which in turn, is directly related to the discharge of the main channel).

Table 4. Summary of Aerial Imagery Interpretations

Site	May 2	May 26	June 7	June 26
Beaver wetland	Flooded	Draining	Half capacity	Half capacity
Side channel	Two channels	One channel	One channel	One channel
Meadow	Yellow	Patchy green	Green	Green

Trends

There are two main trends seen in the aerial imagery of the study site (Table 4, Figures 15 and 16). Firstly, there is a pattern of increasing greenness. In the May 2nd imagery, the meadow is completely brown and yellow. The only greenness in the photo comes from evergreen trees. By May 26th, grass can be seen sprouting spottily all across the meadow, producing a patchy green and yellow-brown mosaic. Additionally, shrubs and non-evergreen trees that were still dormant at the beginning of May have turned green again. This suggests a re-initiation of transpiration as plants begin growing and photosynthesizing again. This greenness increases into June, when it appears to peak. The aerial photos collected on June 7th and June 26th are very similar.

There are patches in the meadow that seem to remain yellow-brown all season. This may be due to laterally variable soil composition and thickness, as well as topographical differences across the floodplain. Also, meadow greenness is most intense right along the banks of the side channel, likely related to the increased water availability along this band.

The second trend visible in the aerial photography is a declining water level. Peak discharge at Taneum Creek is snowmelt-dependent and thus occurs in April. In the May 2nd imagery, the recent presence of floodwaters is apparent. At this time, the side channel is multi-threaded, and water seems to be trapped and ponded in several locations across the floodplain. Filled by floodwaters, the beaver wetland is at its greatest extent. By May 26th, discharge has reduced sufficiently that flow is confined to a single side channel. A corresponding slight water level decline can be seen in the beaver wetland, as its waters are supplied by the side channel. The water level in the beaver wetland continues to decline into June.
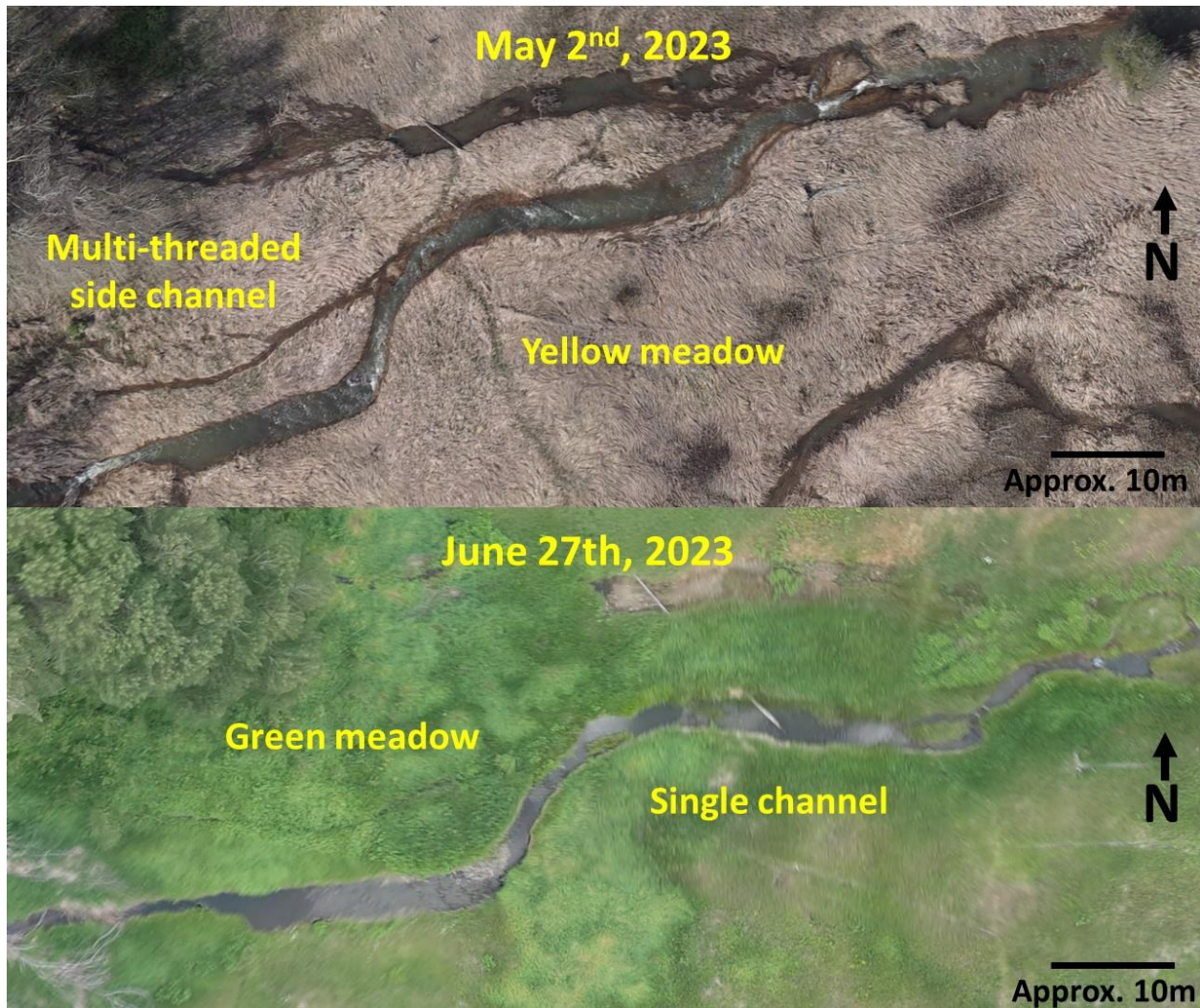
Figure 15. This figure presents a closer look at the Taneum Creek side channel at two different points in time. The above photo shows the area on May 2nd, 2023, when discharge at Taneum is near its yearly highest. At this time, the side channel possesses multiple threads, as snowmelt-fueled discharge flows through the system. The yellow-brown color of meadow grass and general lack of greenery indicates that vegetation is still dormant. The lower photo shows the same area approximately two months later. By this point, flow has reduced such that a single channel is sufficient to drain it. Vegetation has exited winter dormancy and become green again, indicating new growth. The green color seems to be most intense right along the banks of the side channel, likely due to locally increased water availability.
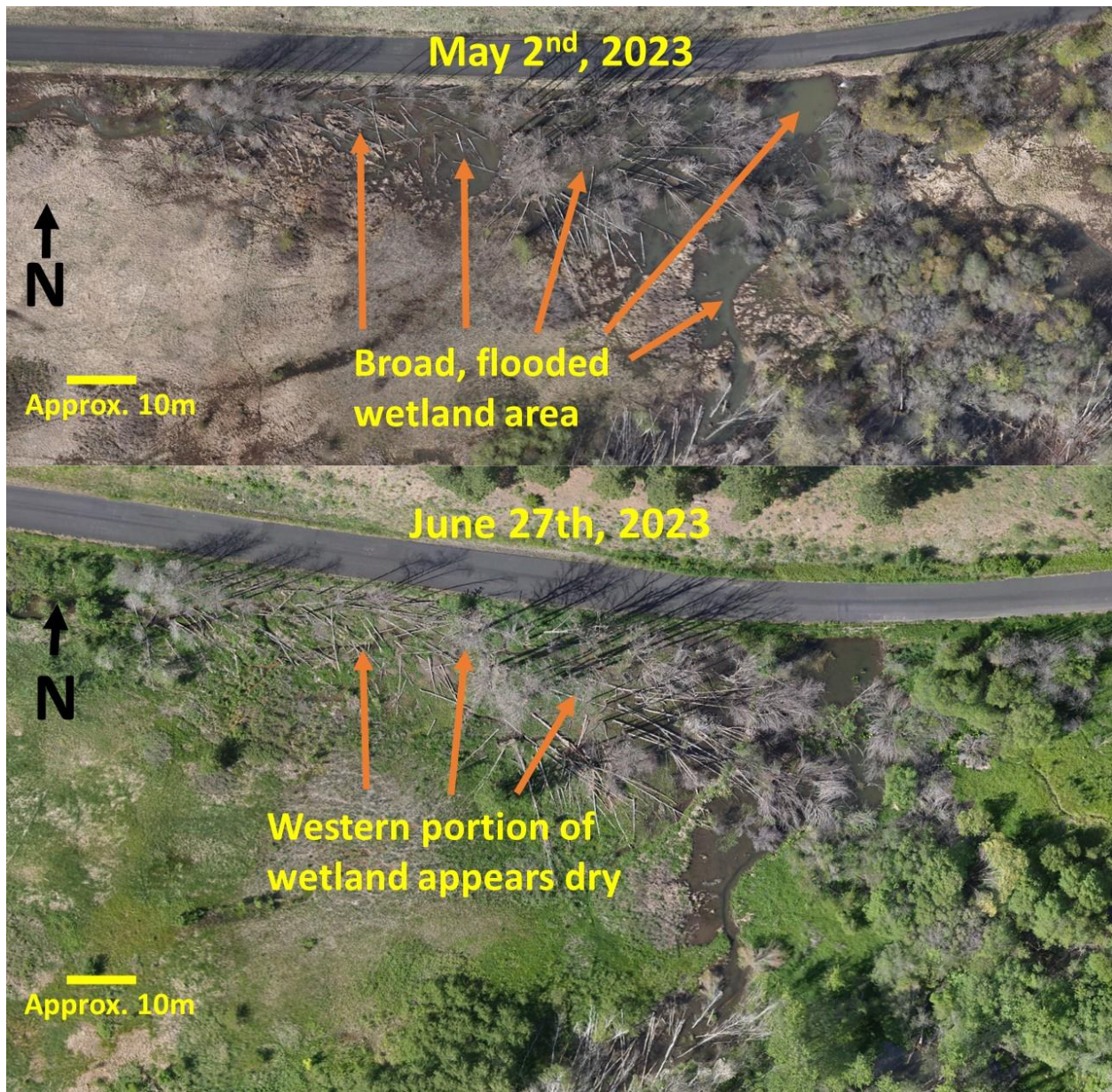
Figure 16. This figure presents a closer look at the beaver wetland located downstream of the side channel, showing the area at two different times. The upper photo shows the area on May 2nd, 2023, when discharge at Taneum is near its yearly highest. The lower photo shows the same area on June 27th, 2023, approximately two months later. The broad wetland area seen in the earlier image can be seen to be greatly reduced by the time of the second photo. Vibrant new vegetation seems to have overtaken previously flooded portions of the wetland, suggesting that the water table is still likely close to the surface there.

Direct Measurement of Soil Moisture

Soil moisture at both monitoring locations demonstrates a decreasing trend with time, corresponding to the relatively arid conditions of the summer dry season. A more significant decline in water content is seen at the riparian location, even though both sites begin at approximately the same moisture level. Overall, water content seems to fluctuate more significantly closer to the surface than at greater depths, likely because soil nearer to the surface is closer to the recharging effect of infiltrating precipitation. A summary of soil moisture data can be found in Table 5. To aid in interpretation, a comparison of volumetric water content values to qualitative descriptions of soil moisture have been provided in Table 6.

Table 5. Soil Moisture at Depth - Ranked (1st = most moisture)

Riparian (wet) Site	5cm	10cm	15cm	20cm
Start	1st	2nd	3rd	4th**
End	2nd	3rd	1st	4th**
Meadow (dry) Site				
Start	1st*	1st*	2nd	3rd
End	4th	2nd	3rd	1st

*Moisture levels at 5 cm and 10 cm depth at the meadow site were virtually equivalent at the beginning of the monitoring period (6/3/2023 – 7/6/2023)
**Low moisture readings at 20 cm depth at the riparian site are likely a result of poor soil-sensor contact.

Table 6. Volumetric Water Content Interpretation Guide

Value Range	Soil Qualitative Description
>0.3	"Wet to saturated"
0.1 to 0.3	
0 to 0.1	"Oven-dry to dry"

While one may expect to see a gradient of increasing/decreasing water content with depth, the trend is not so simple and linear (Figure 17). At the relatively wet riparian monitoring location in the beginning of the study period, soil moisture is greatest at a shallow 5cm depth. By the end of the study period, water content appears highest at the 15cm depth. A similar trend can be seen at the relatively dry meadow location, where water content is lowest at the 5cm depth by the end of the study period, even though this is the wettest depth at the start of the study period.

At the riparian location, soil moisture at the 20cm depth remains significantly below what it is at other depths for the entire duration of the study, likely due to poor soil-sensor contact. In contrast, at the meadow location, the 20cm depth transitions from being the driest measured depth, to the one holding the most moisture. Overall, soil moisture patterns vary significantly between the two equipment sites.

During the study period, there were two precipitation events, highlighted in green in Figure 17. The first of the precipitation events was relatively minor, occurring during June 11-12th and totaling 6.40mm. While this rain produces a distinct spike in soil moisture at the riparian monitoring location, the corresponding peak at the meadow location is hardly noticeable. The second precipitation event occurred on June 25-26th

was greater, totaling 13.00mm, and occurred over a shorter period. This rain event produced a much greater soil moisture response than the rains earlier in the month at both environmental monitoring sites, likely related to the increased precipitation volume and intensity.

Within the floodplain, soil moisture seems to respond less to infiltration of precipitation with increasing depth. Beyond a 15cm depth, soil moisture remains relatively constant with time, and does not respond significantly to precipitation events. This trend is particularly evident with the flat soil moisture trend seen at a 20cm depth at both monitoring sites.

Interestingly, soil moisture appears to be greater overall at the relatively dry meadow location than the relatively wet riparian location. While at the beginning of the monitoring period, both sites start with comparable levels of soil moisture, by the end of the study period that is no longer true. By the beginning of July, soil moisture is greater at the meadow location than the riparian location at every measured depth. This moisture pattern was unexpected, as the meadow monitoring location is further from the recharging effect of the nearby stream channels than the riparian monitoring location.

The two sites differ in soil depth and composition, particularly grain size. Though no quantitative grain size analysis was conducted, sediment at the riparian location was observed to be noticeably coarser during equipment installation, ranging from fine sand to gravel. In contrast, the meadow sediment is much finer, ranging from clay to coarse sand. This variability in soil composition may have an influence on this unexpected moisture trend.
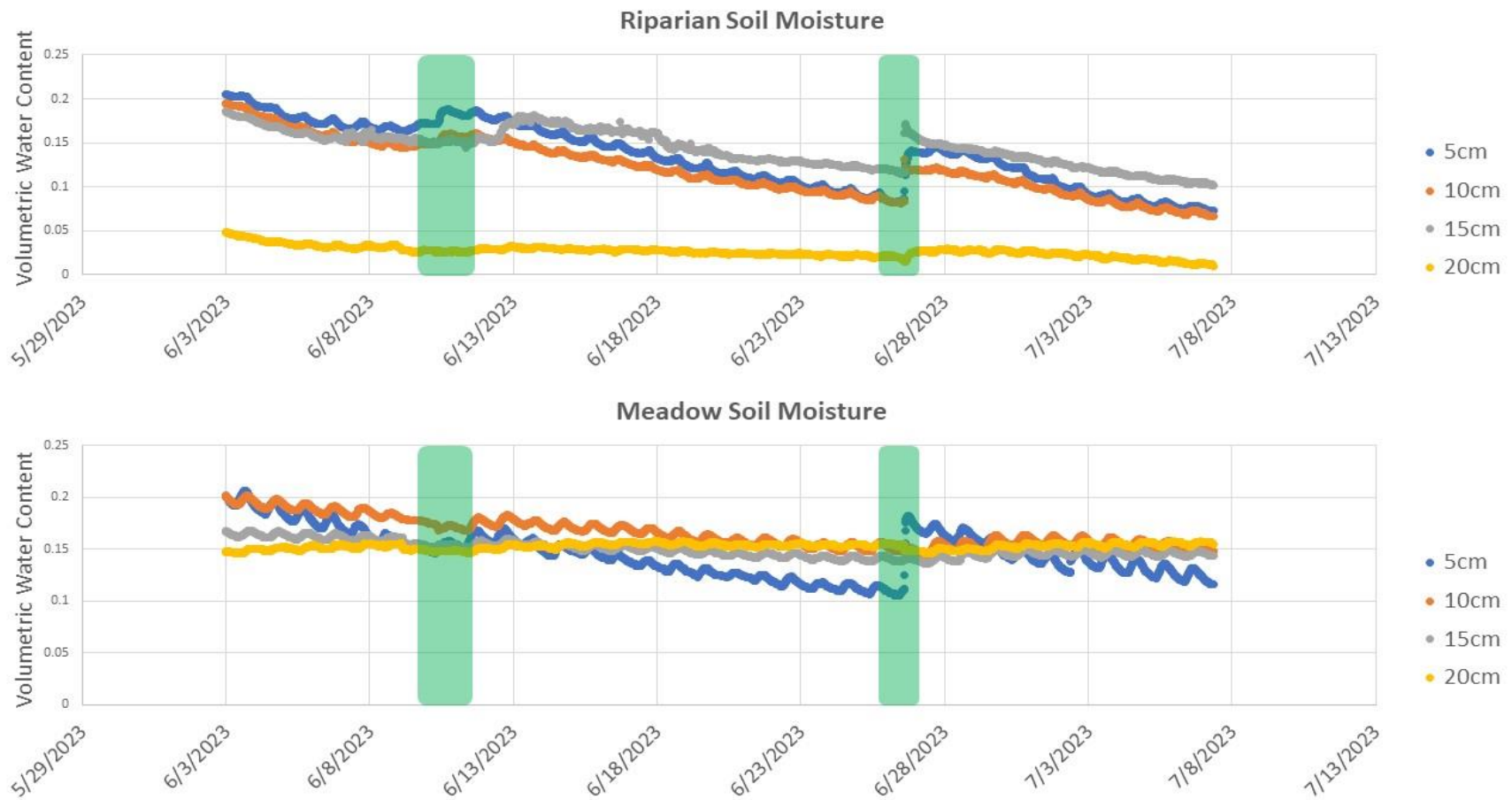
Figure 17. All soil moisture data collected at the two monitoring sites between June 3rd, 2023, and July 7th, 2023. Highlighted in green, the spikes in soil moisture seen around June 12th and June 26th correspond to local precipitation events and associated infiltration. Precipitation on these two days was 6.4mm and 13.0mm respectively. The increase in soil moisture is much greater following the latter precipitation event than the former, likely relating to the difference in precipitation quantity and intensity. The two sites display different temporal and spatial patterns of soil moisture, though they are close in proximity.

45

Alternatively, the meadow monitoring location noticeably lacks vegetation. There are numerous patches across the Taneum floodplain that possess much less vegetation than the surrounding area. The meadow monitoring location was established in one of these relatively clear patches of ground. This lack of flora may limit evapotranspiration at the site to just soil evaporation. Without plants to transpire, water loss over time would be diminished.

Soil Heat Flux (G)

Soil heat flux, G, is the only directly measured Penman-Monteith equation input parameter that varies between the riparian and meadow monitoring locations. The relatively dry meadow monitoring location is surrounded by almost exclusively grass, whereas the relatively wet riparian location represents a mix of vegetation, including grass, brushes, and deciduous and evergreen trees. The two sites are in relatively close proximity to each other, less than 50 m apart. Thus I make the assumption that they are subject to approximately the same weather conditions, though there is likely some variability due to the difference in vegetation and cover between the two sites. Though one may expect net radiation to differ between the two monitoring locations, this is not the case because this parameter is measured at the crop-air interface. Besides soil heat flux, weather-based parameters serve as all the other input variables in the Penman-Monteith equation. As a result, any variation in calculated reference (daily) ET values between the two sites should mirror soil heat flux differences. Daily soil heat fluxes during the entire study period can be seen in Figure 18.
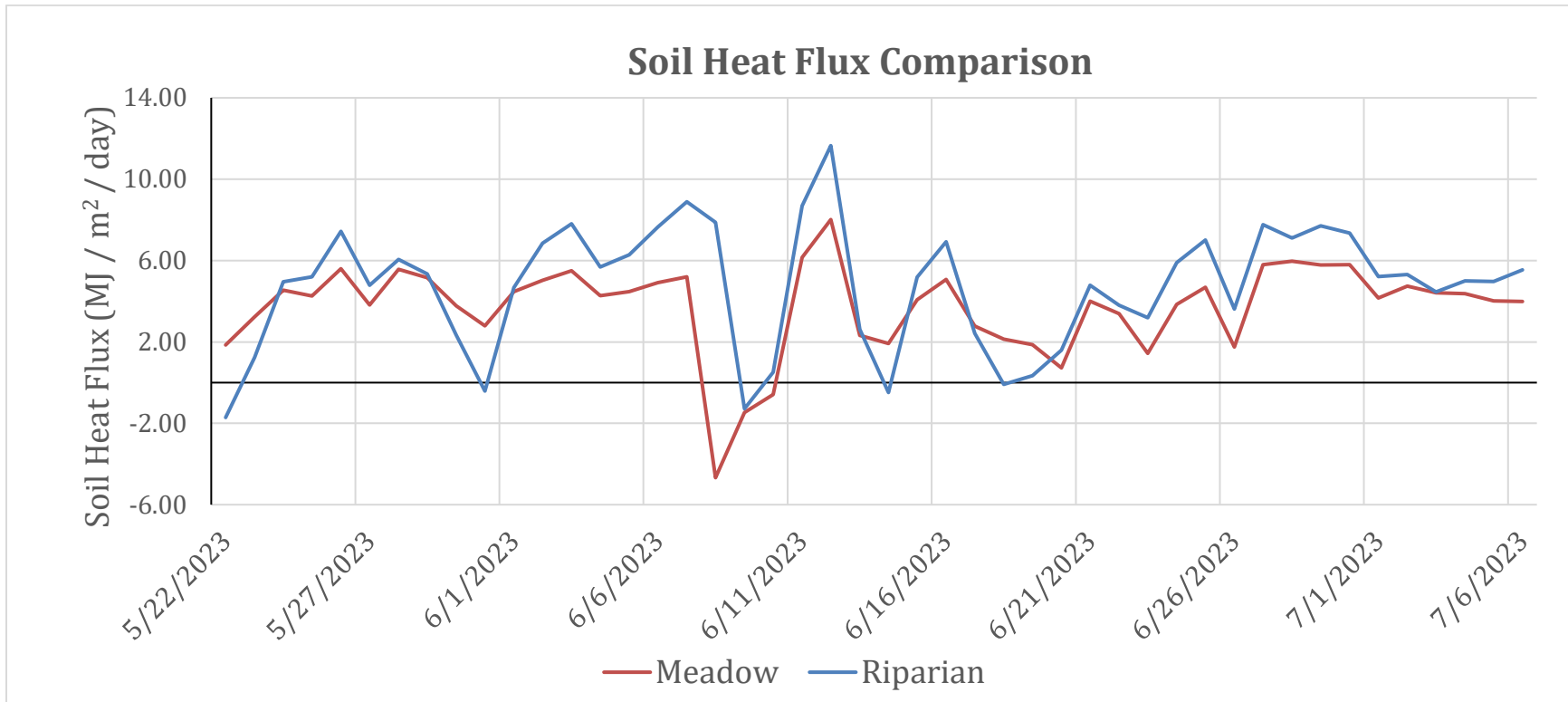
Figure 18. Daily averages of soil heat flux (G) data collected at both monitoring sites. The two sites present similar temporal patterns of G, with the riparian location producing slightly greater values on 83% of days. There are several days where the pattern is flipped, and G is instead greater at the meadow location than the riparian location. These instances include May 22nd, May 31st, June 14th, and June 18th. The unusually low daily average G at the wet site on these days may be related to thermal energy being consumed by the evaporation of morning dew.

The two environmental monitoring sites present similar temporal patterns of G, with the riparian location having higher G on 83% of days. There are several occasions where G is instead greater at the meadow location than the riparian one. These days include May 22nd, May 31st, June 14th, and June 18th. On these days, there are low G totals at the riparian monitoring location. The trend is flipped not because meadow site G is increased, but rather due to low riparian site G values. The anomalously low soil heat flux at the riparian location on these days may be related to thermal energy being consumed by the evaporation of morning dew, rather than penetrating and heating the soil.

This flipped flux pattern is examined more closely in Figure 19, which compares a day in which riparian G is greater to a day in which meadow G is greater. On the few days where the reverse trend is true, and soil heat flux is greater at the meadow location than the riparian one, the daily heat flux total at the riparian location is negative. This indicates a net surface-wards transfer of thermal energy on that day. Upon closer look, instantaneous soil heat flux measurements on the reverse trend days remained negative until 11am-noon. In contrast, on most days, this transition occurs closer to 8am.
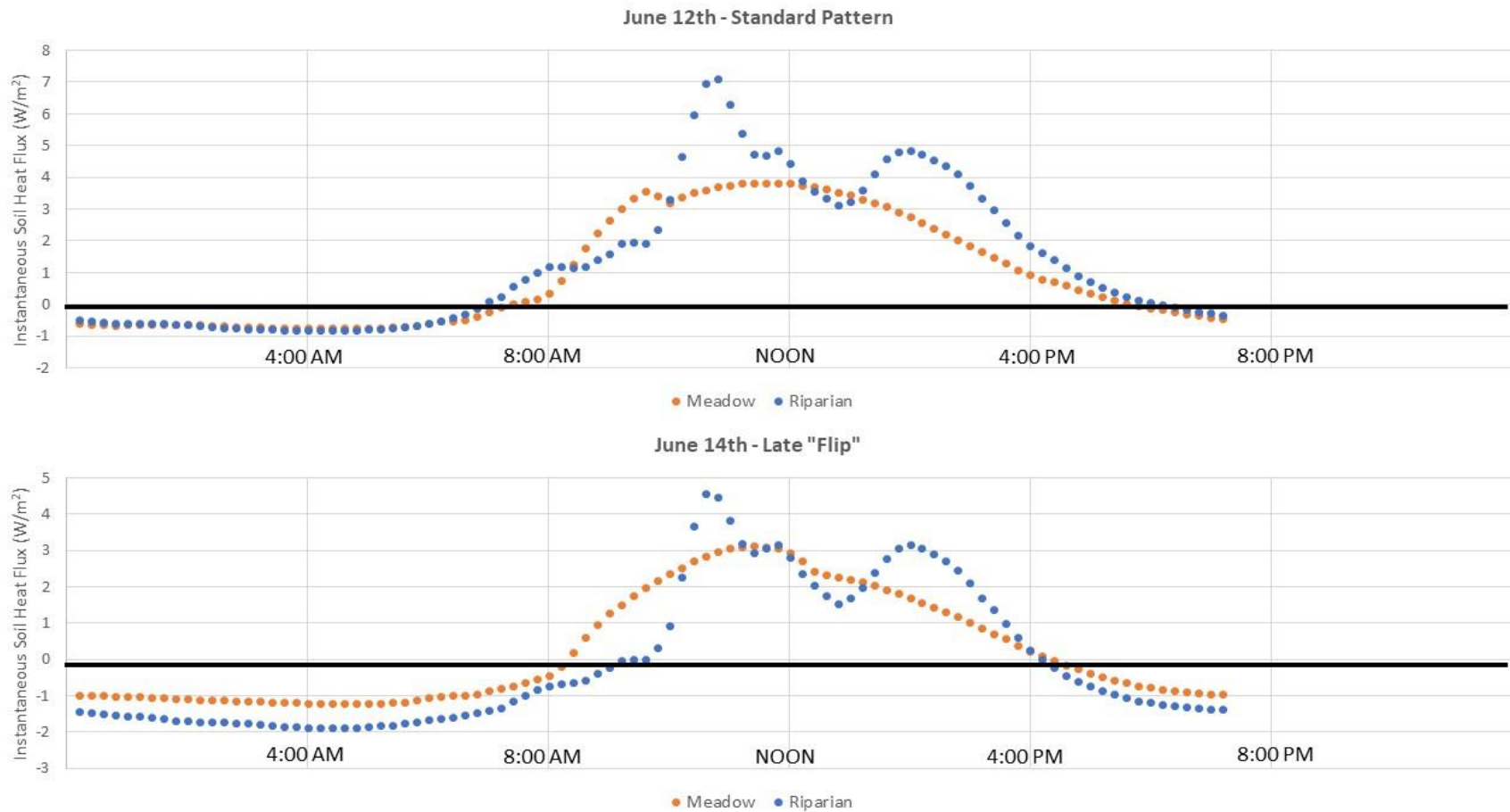
Figure 19. This figure aims to offer an explanation for when the daily heat flux total is greater at the meadow site than the riparian site. On the few days where the "reverse" trend is true, the heat flux total at the riparian location is negative. This indicates net surface-wards transfer of thermal energy. Upon closer look, there seems to be a later "flip" occurring between positive and negative flux values. Instantaneous soil heat flux measurements on these reverse trend days remained negative until 11am-noon, in contrast to the pattern seen on most days, where this transition generally closer to 8am.

A diurnal comparison of instantaneous G fluxes between the beginning and end of the study period at the two sites can be seen in Figure 20. In both 48-hour excerpts, G has greater peaks at the riparian site than the meadow site. Interestingly, the magnitude of peak values is comparable, even though the two time periods have different weather conditions, particularly temperature. This seems to indicate that the limiting factor in soil heat flux may be the physical properties that dictate its ability to conduct heat, rather than air temperature or intensity of solar radiation. The immense insulative effect of soil seems to be limiting soil heat flux magnitude.

Unlike the nice round peaks seen with the meadow location's G data, the riparian location consistently displays a distinctive double-peaked pattern. This pattern is likely associated with sun and shade patterns throughout the day. In contrast to the singular and dominant meadow grass present near the meadow location, monitoring equipment at the riparian location is surrounded by taller vegetation, including brushes and deciduous and evergreen trees (Figure 14).
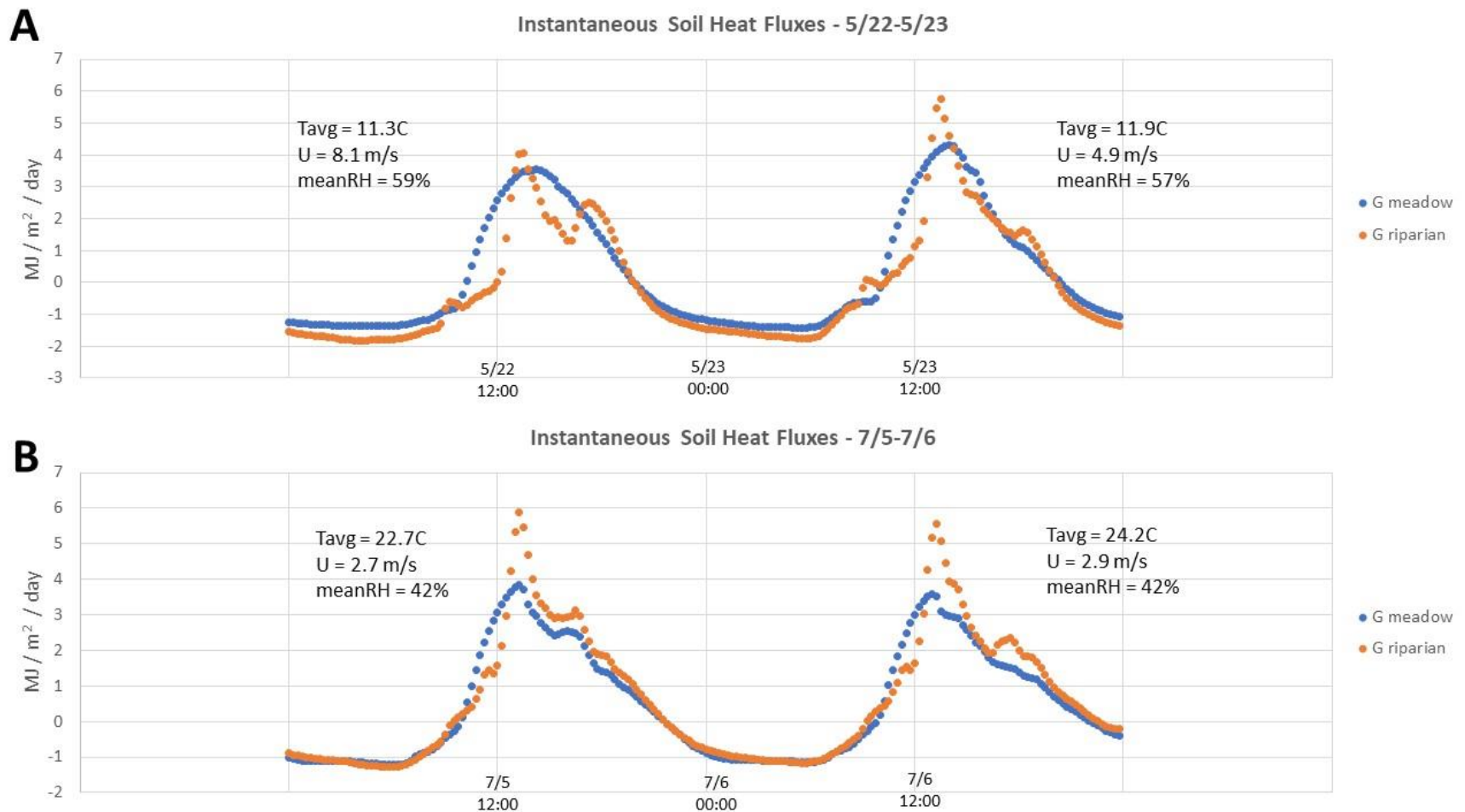
Figure 20. This figure aims to examine diurnal trends in soil heat flux (G) by comparing data from the first two (A) and last two days (B) of the study period. The wet site displays a distinctive double peaked pattern, which is likely associated with sun and shade patterns. In contrast to the dominant and ubiquitous grass present at the meadow location, the riparian site is surrounded by taller vegetation, including brushes and trees.

Pan Evaporation

Using pan evaporation as a proxy is a common method of quantifying evaporation. Evaporation pans generally overestimate actual evaporation, because they are relatively shallow and can be heated from the sides and bottom as well as the top, so evaporation rates are corrected using a pan coefficient (Allen et al., 1998). Derived from local wind speed and relative humidity data, pan coefficients ranged from 0.48 to 0.71. The average of all daily pan coefficients during the measurement period (May 26th to July 6th, 2023) is 0.59. A visual summary of all pan data is shown in Figure 21.
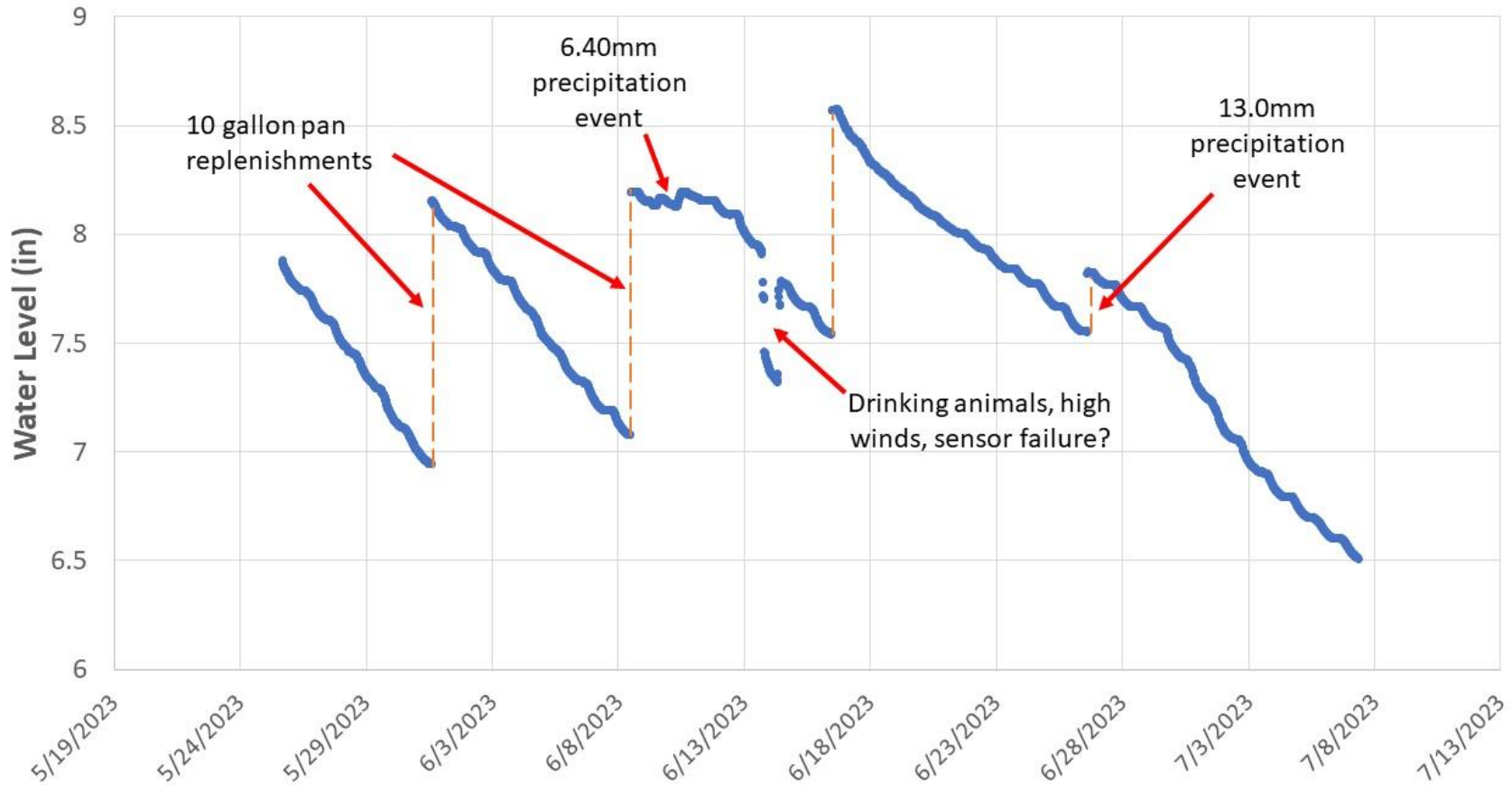
Figure 21. Summary of all evaporation pan data collected between May 25th, 2023 and July 7th, 2023. The pan was manually refilled on May 31st, June 9th, and June 16th, with approximately 10 gallons of water from the Taneum Creek main channel. There was also a 6.4mm precipitation event during June 13th-14th, and a 13.0mm precipitation event during June 26th-27th, which raised the pan's water level. The sudden drop and recovery in water level on June 14th is likely due to sensor error.

53

Penman-Monteith Determinations of Evapotranspiration

Reference ET for both environmental monitoring sites was calculated using a FAO-56 form of the Penman-Monteith calculation adapted from Zotarelli et al. (2010). A summary of ET calculation results can be seen in Figure 22. Daily measured input values to the Penman-Monteith equation can be found in Appendix A.

On most days, daily ET between the two equipment sites is very similar. There is one day during the study period where the difference in reference ET between the two equipment sites is greater than 1mm: June 9th. On this day, ET for the meadow location spikes dramatically. There is a similar spike in ET at the riparian location, but it is delayed and of lesser magnitude.

During the period of June 8th and 9th, there was a significant and extended summer storm event occurring in the Kittitas Valley, which produced 6.4mm of rainfall. The combination of precipitation, cool temperatures, and reduced solar radiation on these two overcast days may be responsible for the sudden spike in ET at the meadow monitoring location.

However, these ET values may be overestimations, due to the limited vegetation present at the meadow location. It takes time and resources for vegetation to establish; it generally does not appear overnight after a single storm event. Though after the storm environmental conditions may have been favorable for increased transpiration, there was not necessarily established vegetation ready to take advantage of the increased resource availability.
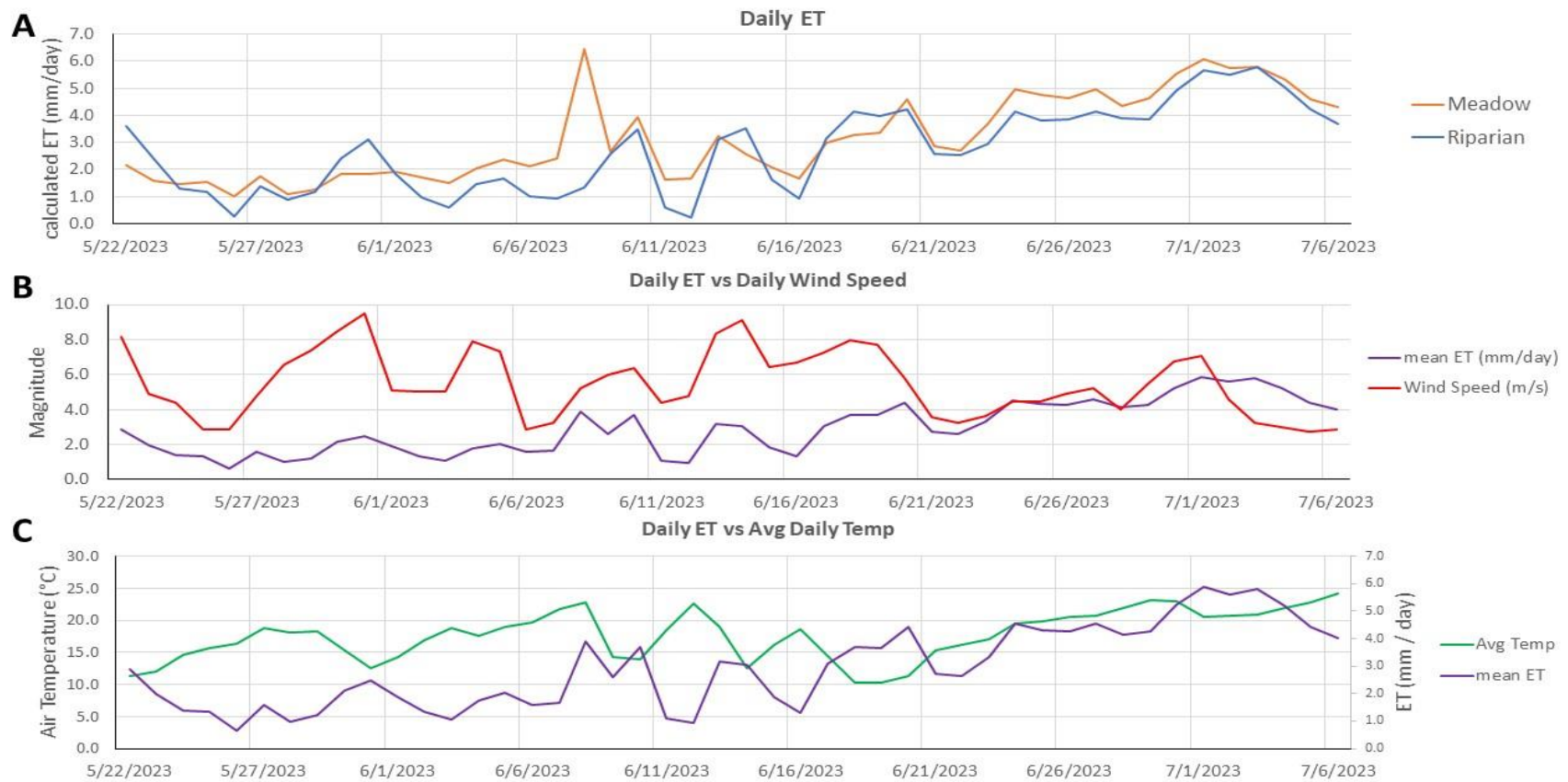
Figure 22. This figure shows temporal trends for calculated reference ET, and how these values relate to average daily temperature and wind speed. **A** compares reference ET between the relatively dry "meadow" and relatively wet "riparian" monitoring sites. Excluding the outlier data point that produces a peak in meadow location ET on June 8th, the two monitoring sites demonstrate similar values and temporal patterns in ET. **B** compares mean ET (average of both locations' reference ET) with daily average wind speed. During the first half of the study period, mean ET and average daily wind speed appear highly correlated. However, this trend seems to terminate at the end of June. **C** compares mean ET to average daily temperature. Though there appears to be some correlation between these final two parameters, their relationship is certainly complex.

55

ET seems to have a slight positive correlation with wind speed. When wind speed increases, evapotranspiration increases to match. Air movement plays a significant role in regulating relative humidity, and can directly affect rates of evaporation and transpiration. Greater wind speeds can enhance the rate of evaporation from the surfaces of water bodies, soil, and vegetation. The movement of air across these surfaces removes the saturated air layer close to the surface, allowing more moisture to evaporate. Thus, as wind speed increases, the evaporation rate generally rises. Additionally, wind generates turbulence in the air, leading to better mixing and dispersion of water vapor. This turbulence increases the rate of evaporation by exchanging moist air near the surface with drier air from above, resulting in an accelerated evaporation process (Rana & Katerji, 2000).

Similarly, for plants, wind can increase the rate of transpiration. When the wind blows across leaves, it can cause an increase in the rate of water vapor diffusion from the stomata (pores) on the leaf surfaces. This enhanced diffusion promotes higher transpiration rates, leading to increased water loss from plants (Rana & Katerji, 2000). Strong winds can lead to a drying effect by removing moisture from the surrounding environment. As wind speed increases, it carries away the moist air from the vicinity of the evaporating surface, maintaining a lower humidity level around it. This reduction in humidity gradient enhances the evaporation rate (Rana & Katerji, 2000).

There also appears to be a correlation between ET and air temperature. Like air movement, air temperature plays a significant role in influencing and regulating ET (Rana & Katerji, 2000). In this study, there is a trend of ET increasing as average daily

air temperature decreases. However, this relationship is not as clear as between ET and wind speed. Generally, greater air temperature seems to be associated with greater potential rates of evapotranspiration. The greatest potential ET values are generally seen in July, which are also when all the warmest days during the study period occur.

Air temperature may affect rates of ET in a variety of ways. As the temperature rises, the kinetic energy of water molecules also increases, causing more molecules to transition from a liquid to a gaseous state. This increased energy accelerates the evaporation process from surfaces such as water bodies, soil, and plants. Additionally, warmer air can hold more water vapor. As the temperature rises, the air has a greater capacity to hold moisture. This increased capacity creates a larger vapor pressure gradient between the surface and the air, facilitating faster evaporation. Crucially for ET, air temperature plays a crucial role in determining the vapor pressure deficit, which is the difference between the saturation vapor pressure and the actual vapor pressure in the air. Higher temperatures lead to increased saturation vapor pressure, while the actual vapor pressure remains relatively constant. This larger vapor pressure deficit enhances the driving force for evapotranspiration (Allen et al., 1998; Allen et al., 2005).

Reference ET Estimate Comparisons

Comparisons of daily ET from different methods can be found in Figure 23. The data used to generate this plot can be found in Appendix B. Calculated average rates of ET across the whole study period (May 22nd, 2023 through July 6th, 2023) can be seen in Figure 24. In the first half of the study period, my empirically calculated reference ET values are greater than 100% less than the estimates produced by the ensemble of models used by OpenET. By the latter half of the study, that discrepancy is much less but remains visible. In general, the estimates derived from OpenET are more constant over time than the empirically derived estimates, which increase between May and July. ET estimates by OpenET range from 4-7 mm/day (OpenET, 2023), whereas my estimates range from almost 0 mm/day to as much as 6.5 mm/day. This difference may be related to the timeline of vegetation growth at Taneum. Though water may be available early, dormant perennial plants need time to reactivate their metabolism and take advantage of the increased resource availability. Similarly, fresh annual plants need time to sprout and establish before they can begin photosynthesizing and evapotranspiration at greater rates.

Overall, my estimates of reference ET for the Taneum meadow are consistently lower than the values generated by OpenET. This is particularly true during the windows of May 24th to June 7th and June 12th through June 16th. The only days on which the OpenET estimate is lower than my empirical estimates are June 9-10th, and June 20th. These were both periods with abnormally low mean daily temperatures. On June 9th and 10th, the mean daily temperature was only 14°C, in contrast to the 22°C seen on

June 7th and 8th, just two days prior. Similarly, the average daily temperature on July

18-20th is only 11°C. OpenET's estimates of ET rely on long-wave thermal satellite

imagery, and are thus likely greatly influenced by air temperature (OpenET, 2023).

Additionally, my Penman-Monteith determinations of ET may fail to account for the

immense role of the many cottonwood (*Populus fremontii)* trees present at Taneum,

which are known to have a particularly high rate of ET. As an example, a study of a

cottonwood plantation in Arizona quantified the transpiration rate of these trees at 1.2m

per year (Nagler et al., 2007).
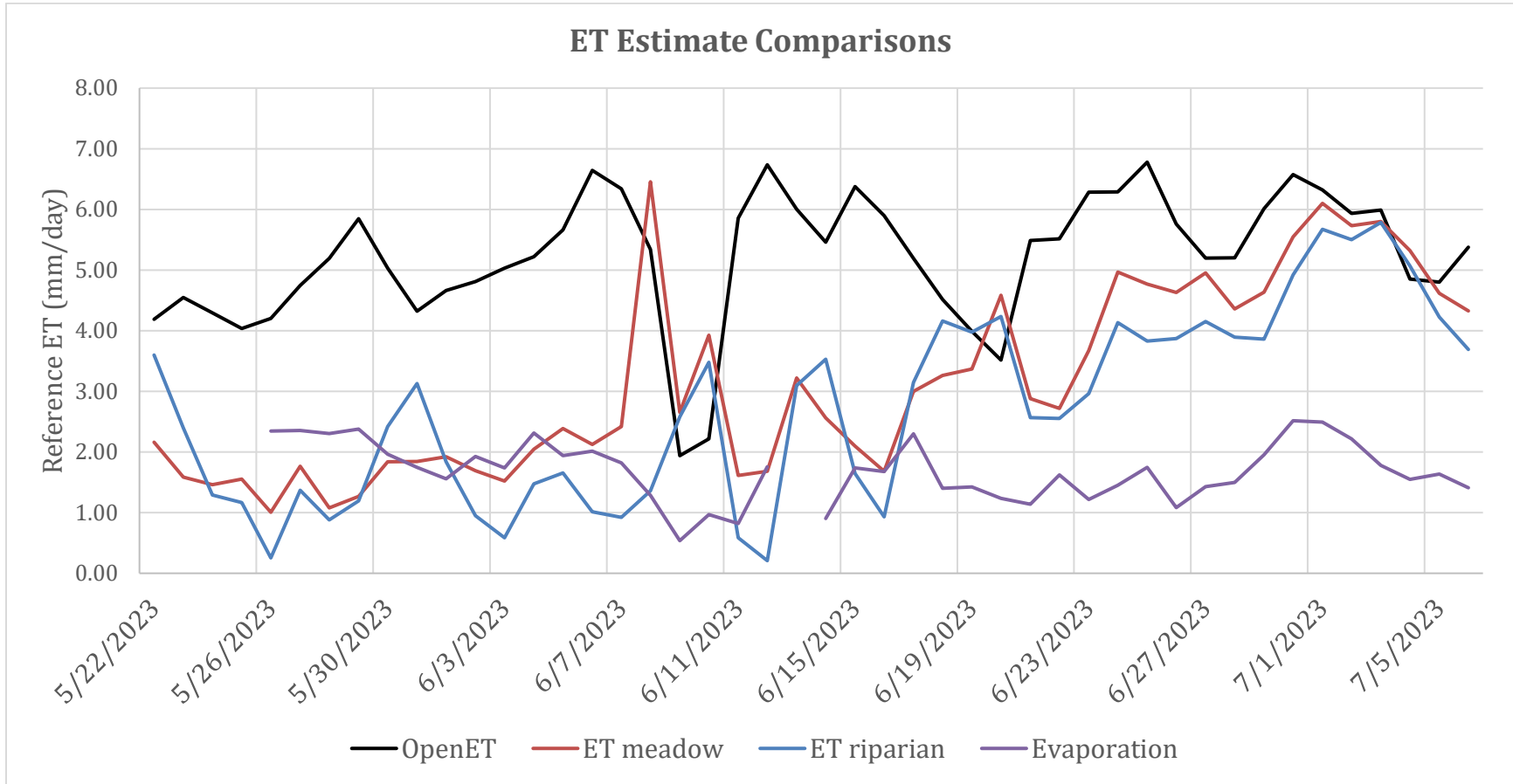
Figure 23. Visual comparison of all ET estimates produced in this study. The orange and gray lines display daily reference ET values calculated via the Penman-Monteith equation for the "dry" and "wet" environmental monitoring sites respectively. The blue line represents the mean estimate produced by OpenET's collection of remote-sensing based models (OpenET, 2023). The yellow line displays pan evaporation, which has been averaged across the whole study period. Empirical estimates of ET (dry and wet sites) demonstrate an increasing trend with time. The trend in OpenET's estimates of ET is relatively flat in comparison. Pan evaporation is greater than empirical measures of ET for the first half of the study, but this relationship flips by June 20th.
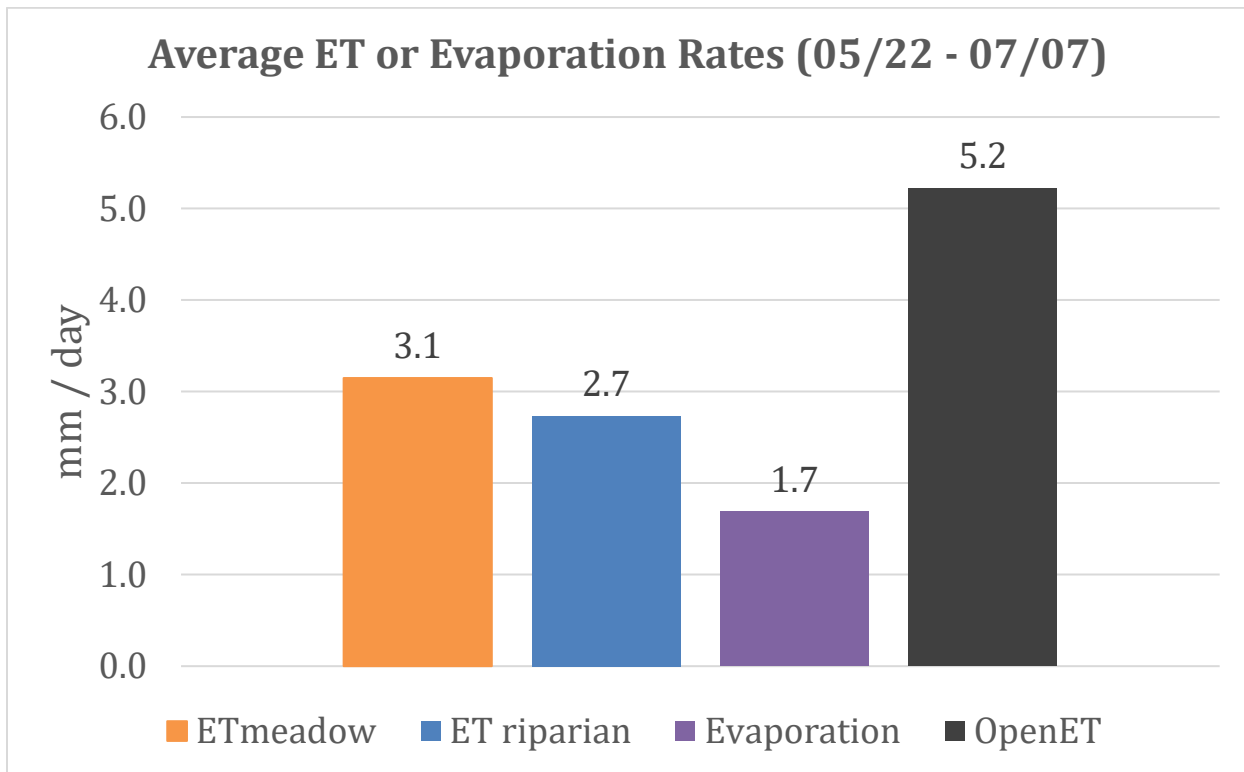
Figure 24. This figure compares the average rates of water loss during the whole study period to each other. In comparison to the empirically derived rates, the OpenET data is much greater. By subtracting the rate of pan evaporation, water loss by transpiration can be isolated. These isolated transpiration rates are 1.4 mm/day (ET meadow), 1.0 mm/day (ET riparian), and 3.5 mm/day (OpenET).

Comparison of Total ET Estimation with Floodplain Storage

A recent estimate by Polizzi (2023) quantifies the floodplain area of the Taneum Creek watershed as between 587 and 693 acres. These estimates were generated through a combination of field work, mapping, and grain-size analysis. These values can be used to calculate the volume of water that is lost to ET by multiplying by the total ET (in feet) during that time (Table 7).

Table 7. Calculated Water Loss Volumes for Taneum Floodplain (5/22/2023 - 7/6/2023)

Reference Rate	Sum ET (ft)	Low Estimate (acre-ft)	High Estimate (acre-ft)
ET meadow	0.475	279	329
ET riparian	0.413	242	286
OpenET	0.788	463	546
Evaporation	0.300	176	208

Here we use the units of acre-ft for volumes, because they are standard among water managers in the US.

Polizzi also quantified the total floodplain aquifer capacity for Taneum Creek. However, their analysis examines only the top 1-2 meters of floodplain soil, beneath which is a confining clay layer that functions as an aquitard. Their estimates range from as little as 352 acre-ft to as high as 1,320 acre-ft (Polizzi, 2023).

ET data generated via the Penman-Monteith method suggests that a significant volume of the floodplain aquifer's water is consumed during the summer dry season by evapotranspiration (Table 8). Assuming Polizzi's lowest volume estimate of 352 acre-ft, anywhere from 69% to 93% of the aquifer's capacity is lost by ET in six weeks. If we are to use Polizzi's greatest volume estimate, those percentages become 18% to 25%. The aquifer is not receiving recharge from precipitation at this time, but this large outflow suggests that there is recharge from the river and/or the underlying aquifers during this period. It is also possible that some of this ET loss is from a deeper part of the alluvial aquifer, below the confining clay layer which Polizzi (2023) used as the lower limit of the unconfined floodplain aquifer.

The pan evaporation data, which excludes transpiration related water loss, displays the lowest volume of water loss. Pan data indicates that between 50% and 59% of Polizzi's lowest capacity estimate and 13% and 16% of her highest estimate is consumed by evaporation.

Table 8. ET Estimates during 5/22-7/6 as Percentage of Total Aquifer Capacity

Estimate Type	Lowest Capacity (352 acre-ft)	Highest Capacity (1320 acre-ft)
ET meadow	79-93%	21-25%
ET riparian	69-81%	18-22%
OpenET	131-155%	35-41%
Evaporation	50-59%	13-16%

CHAPTER V

CONCLUSION

Taneum Creek is a tributary in the upper Yakima River basin, located in central

Washington state in the rainshadow of the Cascade Mountains. This study aimed to

quantify ET water loss from Taneum Creek and its floodplain during the dry season,

when stream flows are maintained by groundwater baseflow.

Extensive restoration efforts on Taneum Creek, primarily through large wood

emplacement, have greatly increased channel-floodplain connectivity and returned the

hydrology and geomorphology to a more "natural" state. This has had beneficial impacts

on the wildlife in the area, especially spawning fish. Since restoration, beavers have

colonized the area. Their ecological engineering has further altered surface and

groundwater flows at the study site. In general, the increased connectivity and beaver

activity has led to a greening of the floodplain and increased recharge of the floodplain

aquifer through side channels and overbank flows. However, the increased vegetation

growth can in turn remove water from the floodplain aquifer at a greater rate through ET

and the net impact of restoration on aquifer storage depends on this balance.

For this study, soil moisture was monitored directly at two different locations in

the floodplain, representing the relatively moist riparian zone and the drier meadow

nearby. Overall, soil moisture at both sites demonstrates a decreasing trend with time,

corresponding with the relatively arid conditions of the summer dry season. Additionally,

soil moisture fluctuates more broadly closer to the surface than at greater depths.

Beyond a 15cm depth, soil moisture remained relatively constant with time, and did not

respond significantly to precipitation events. Interestingly, soil moisture content was slightly higher at the meadow site than the riparian site. This unexpected pattern may be explained by differences in soil texture.

A range of daily evaporation and ET rates were calculated based on pan evaporation, soil heat flux measurements. The soil heat flux calculations were based on a surface energy balance (Penman-Monteith method). These calculated evaporation and ET values were compared to publicly available satellite-based ET estimates from the platform OpenET. OpenET presents data from multiple models which also employ a surface energy balance approach. For the Taneum Creek site, the OpenET estimates of ET are consistently in the range of 4-7 mm/day (OpenET, 2023). At the start of the period, these estimates were greater than 100% more than the Penman-Monteith ET determinations, though by the end of the study this difference is much reduced. ET from larger trees in the floodplain such as cottonwoods may explain this discrepancy. The Penman-Monteith calculations of ET demonstrated an increasing trend with time, starting at about 2 mm/day on May 22nd, and increasing to about 4 mm/day by July 7th. The difference in ET estimates between the two monitoring locations was not statistically significant. Evaporation calculated from pan evaporation, which excludes transpiration, displayed the lowest rate of water loss, at an average of 2 mm/day across the study period. Isolated transpiration rates were calculated by subtracting the evaporation component from ET estimates. These rates are 1.4 mm/day for the "dry" soil location, 1.0 mm/day for the "wet" soil location, and 3.5 mm/day for OpenET.

Daily reference ET values were compared to recent estimates of floodplain aquifer capacity for Taneum Creek developed by Polizzi (2023). Polizzi (2023) estimated that the floodplain aquifer volume in the study area ranged between 352 and 1320 acre-ft. ET data generated via the Penman-Monteith method suggests that a significant volume (242-329 acre ft) of the floodplain aquifer's water is consumed in just six weeks (05/22/2023 - 07/06/2023). In comparison to the lowest floodplain aquifer capacity value used, these estimates range from 69% to 93% of the total capacity. Assuming the greater floodplain aquifer capacity, the Penman-Monteith ET estimates range from 18-25% of the total capacity. However, it is important to note that Polizzi's capacity estimate only accounts for the upper portion of the floodplain aquifer due to a confining clay layer found at 1-2 m depth.

The dry season at Taneum Creek is much longer than just the six weeks examined in this study. However, by this six-week mark, ET has already consumed a volume of water that is greater than half the volume of lower estimates of floodplain aquifer capacity. While the combination of large wood emplacement, the 100-yr flood of 2011, and beaver activity may have increased channel-floodplain connectivity and maintained groundwater later into the summer, data from this study suggests that any boosts in groundwater storage are likely negated by increased vegetation growth and evapotranspiration. Though the floodplain aquifer may not be an effective reservoir for human use, stream restoration is still undoubtedly an enormous success. It has restored and provided a crucial and invaluable home for a variety of local aquatic wildlife, especially beavers and spawning fish.

REFERENCES

Abbe, T.B. and Montgomery, D.R., 1996, Large woody debris jams, channel hydraulics and habitat formation in large rivers, Regulated Rivers: research & management, no 2-3, p. 201-221.

Aboukhaled, A., Alfaro, A. and Smith, M., 1982, Lysimeters. *Irrigation and Drainage Paper (39).* 69.

Allen, R. G., Walter, I. A., Elliot, R. L., Howell, T.A., Itenfisu, D., Jensen, M. E. and Snyder, R., 2005, The ASCE standardized reference evapotranspiration equation, ASCE and American Society of Civil Engineers.

Allen, R.G.; Pereira, L.S.; Raes, D.; Smith, M. Crop evapotranspiration: guidelines for computing crop water requirements. Rome: FAO, 1998. 301p. Irrigation and Drainage Paper, 56

Buffington, J.M., and Montgomery, D.R., 1999, Effects of sediment supply on surface textures of gravel-bed rivers: *Water Resources Research*, v. 35, p. 3523–3530, doi: 10.1029/1999wr900232.

Butler, D.R., and Malanson, G.P., 1995, Sedimentation rates and patterns in beaver ponds in a mountain environment: *Geomorphology*, v. 13, p. 255–269, doi: 10.1016/0169-555x(95)00031-y.

Cohen, Y., Fuchs, M., Falkenflug, V., & Moreshet, S., 1988, Calibrated Heat Pulse Method for Determining Water Uptake in Cotton, *Agronomy Journal, 80*(3), 398-402. doi:10.2134/agronj1988.00021962008000030004x

Cohen, Y., Takeuchi, S., Nozaka, J., & Yano, T., 1993, Accuracy of Sap Flow Measurement Using Heat Balance and Heat Pulse Methods, *Agronomy Journal, 85*(5), 1080-1086. doi:10.2134/agronj1993.00021962008500050023x

Collins, B. D., Montgomery, D. R., Fetherston, K. L., and Abbe, T. B., 2012, The floodplain large-wood cycle hypothesis: A mechanism for the physical and biotic structuring of temperate forested alluvial valleys in the North Pacific coastal ecoregion. *Geomorphology*, v. 139, p. 460-470.

Collins, B. D., Montgomery, D. R., Schanz, S. A., and Larsen, I. J., 2016, Rates and mechanisms of bedrock incision and Strath Terrace Formation in a forested catchment, Cascade Range, Washington. *Geological Society of America Bulletin*, 128(5-6), 926–943. https://doi.org/10.1130/b31340.1

Comiti, F., Lucía, A. and Rickenmann, D., 2016, Large wood recruitment and transport during large floods: a review. *Geomorphology*, v. 269, p. 23-39.

Dolloff, C.A. and Warren, M.L., 2003, Fish relationships with large wood in small streams, American Fisheries Society Symposium 37: 179-193, 2003.

Ely, D.M., Bachmann, M.P., and Vaccaro, J.J., 2011, Numerical simulation of groundwater flow for the Yakima River basin aquifer system, Washington: U.S. Geological Survey Scientific Investigations Report 2011-5155, 90 p.

Ely, L. and Gazis, C., 2021, Evapotranspiration and Floodplain Aquifer Storage Capacity in Yakima Tributaries, Unpublished research proposal.

Fixler, Samuel, "Decadal-Scale Effects of Large Wood Restoration on Channel Morphology and Groundwater Connectivity, Taneum Creek, WA" (2022). All Master's Theses. 1783. https://digitalcommons.cwu.edu/etd/1783

The Frederick Krueger Collection, 1920, Central Washington University Library Archives, https://digitalcommons.cwu.edu/frederickkrueger/.

Gendaszek, A.S., Ely, D.M., Hinkle, S.R., Kahle, S.C., and Welch, W.B., 2014, Hydrogeologic framework and groundwater/surface-water interactions of the upper Yakima River Basin, Kittitas County, central Washington: U.S. Geological Survey Scientific Investigations Report 2014 5119, 66 p., http://dx.doi.org/10.3133/sir20145119.

Gergel, D. R., Nijssen, B., Abatzoglou, J. T., Lettenmaier, D. P., and Stumbaugh, M. R., 2017, Effects of climate change on snowpack and fire potential in the western USA. *Climatic Change*, no. 2, p. 287-299.

Grebet, P., & Cuenca, R.H. (1991). History of Lysimeter Design and Effects of Environmental Disturbances.

Hanson, R. L., 1991, Evapotranspiration and Droughts, U.S. Geological Survey, https://geochange.er.usgs.gov/sw/changes/natural/et/

Henderson, E.M., 1990, The Pine Tree Express: A history of the Cascade Lumber Company's pine hauling railroad in Kittitas County, Washington, 1916-1946

Johnston, C. A., 2014, Beaver pond effects on carbon storage in soils. *Geoderma*, vol. 213, p. 371-378.

Jones and Stokes Associates, 1991, Watershed characteristics and conditions inventory; Taneum Creek and Tacoma Creek watersheds. Prepared for Washington Department of Natural Resources, p. 61.

Kalma, J.D., McVicar, T.R., and McCabe, M.F., 2008, Estimating land surface evaporation: A review of methods using remotely sensed surface temperature data: *Surveys in Geophysics*, v. 29, p. 421–469, doi: 10.1007/s10712-008-9037-z.

Lewellen, D. G., Walker, C. W., and Cushman, C. D., 1985, Geology and coal potential of the Taneum-Manastash area. Kittitas County, Washington: Washington Division of Geology and Earth Resources Open-File Report, p. 83-9.

Malek, K., Reed, P., Adam, J., Karimi, T., & Brady, M., 2020, Water rights shape crop yield and revenue volatility tradeoffs for adaptation in Snow Dependent Systems, *Nature Communications*, *11*(1). https://doi.org/10.1038/s41467-020-17219-z

McCabe, M.F., Miralles, D.G., Holmes, T.R.H., and Fisher, J.B., 2019, Advances in the remote sensing of terrestrial evaporation: Remote Sensing, v. 11, p. 1138, doi: 10.3390/rs11091138.

McComb, W. C., Sedell, J. R., & Buchholz, T. D., 1990, Dam-site selection by beavers in an eastern Oregon basin. The Great Basin Naturalist, p. 273-281

McKinley, C., and Sandison, D.I., 2012, Yakima River Basin Integrated Water Resource Management Plan: Washington State Department of Ecology 12-12–002.

Meseck, D., 2020, Yakima County Profile. Washington Employment Security Department. https://esd.wa.gov/labormarketinfo/county-profiles/yakima

Monk, P.A., 2015, Steelhead Return to Taneum Creek Following Habitat Restoration. Prepared for U.S. Bureau of Reclamation, Yakima River Basin Water Enhancement Project, prepared by U.S. Fish and Wildlife Service, Mid-Columbia Fishery Resource 61

Monk, P., 2009, Taneum Creek Study: The Bruton-KRD Water Exchange Project. Bureau of Reclamation Open-File Report, p. 1-26

Nagler, P., Jetton, A., Fleming, J., Didan, K., Glenn, E., Erker, J., Morino, K., Milliken, J., Gloss, S., 2007, Evapotranspiration in cottonwood (*Populus fremontii*) restoration plantation estimated by sap flow and remote sensing methods. Agricultural and Forest Meteorology 144: 95-110 DOI: 10.1016/j.agrformet.2007.02.002.

Ohashi, K., Kobayashi, K., Fujii, H., & Watanabe, M., 2020, Evaporation coefficient and condensation coefficient of vapor under high gas pressure conditions, *Scientific Reports, 10*(1). doi:10.1038/s41598-020-64905-5

OpenET, https://openetdata.org/ (accessed July 2023).

Polizzi, Emily, "Floodplain Aquifer Storage Capacity in Upper Yakima River Tributaries, Kittitas County, WA" (2023). All Master's Theses. 1872. https://digitalcommons.cwu.edu/etd/1872

Rana, G., & Katerji, N., 2000, Measurement and estimation of actual evapotranspiration in the field under Mediterranean climate: A review. *European Journal of Agronomy, 13*(2-3), 125-153. doi:10.1016/s1161-0301(00)00070-8

Roni, P., Beechie, T., Pess, G. and Hanson, K., 2015, Wood placement in river restoration: fact, fiction, and future direction. Canadian Journal of Fisheries and Aquatic Sciences, no. 3, p. 466-478.

Russell, I.C., 2016, Rivers of North America: Creative Media Partners, LLC

Schanz, S.A., Montgomery, D.R., and Collins, B.D., 2019, Anthropogenic strath terrace formation caused by reduced sediment retention: Proceedings of the National Academy of Sciences, v. 116, p. 8734–8739, doi: 10.1073/pnas.1814627116.

Subedi, A., and Chávez, J.L., 2015, Crop evapotranspiration (ET) estimation models: A review and discussion of the applicability and limitations of ET methods: Journal of Agricultural Science, v. 7, doi: 10.5539/jas.v7n6p50.

Tabor, R. W.; Waitt, R. B., Jr.; Frizzell, V. A., Jr.; Swanson, D. A.; Byerly, G. R.; Bentley, R. D., 1982, Geologic map of the Wenatchee 1:100,000 quadrangle, central Washington: U.S. Geological Survey Miscellaneous Investigations Series Map I-1311, 1 sheet, scale 1:100,000, with 26 p. text. [http://pubs.er.usgs.gov/usgspubs/i/i1311/]

Tanner, C.B.,1967, Measurement of evapotranspiration, *Irrigation of Agricultural Lands (11). 534-574.*

Tappel, P., 2012, Consideration of Large Wood Placed in Taneum Creek by the Yakima Indian Nation, with Respect to Flood Damages to Private Property in Mid-May 2011. Fisheries Engineers, Inc Open-File Report, p. 1-8

Toth, S, 1995, In Support of the Habitat Conservation Plan on Forested Lands Owned by Plum Creek Timber Company, L.P. in the I-90 Corridor of the Central Cascades Mountain Range, Washington, 1995. Technical Report #11

U.S. Department of the Interior Bureau of Reclamation Pacific Northwest Region and State of Washington Department of Ecology Central Regional Office, 2012, Yakima River Basin Integrated Water Resource Management Plan Final Programmatic Environmental Impact Statement BENTON, KITTITAS, KLICKITAT AND YAKIMA COUNTIES, Ecological Publication Number: 12-12-002:

https://www.usbr.gov/pn/programs/yrbwep/reports/FPEIS/fpeis.pdf, (accessed June 2023).

Vaccaro, J. J., Jones, M. A., Ely, D. M., Keys, M. E., Olsen, T. D., Welch, W. B., & Cox, S. E, 2009, Hydrogeologic framework of the Yakima River Basin Aquifer System, Washington, Scientific Investigations Report, https://doi.org/10.3133/sir20095152

Vaccaro, J. J., & Olsen, T. D., 2007, Estimates of ground-water recharge to the Yakima River Basin Aquifer System, Washington, for predevelopment and current land-use and land-cover conditions. USGS Scientific Investigations Report 2007-5007, https://pubs.usgs.gov/sir/2007/5007/figure5.html (accessed February 2023).

Vano, J. A., Scott, M. J., Voisin, N., Stöckle, C. O., Hamlet, A. F., Mickelson, K. E., Elsner, M. M. G., & Lettenmaier, D. P., 2010, Climate change impacts on water management and irrigated agriculture in the Yakima River Basin, Washington, USA. *Climatic Change*, *102*(1-2), 287–317. https://doi.org/10.1007/s10584-010-9856-z

Washington State University AgWeatherNet, https://weather.wsu.edu/?p=92850&desktop (accessed July 2023).

Whiteway, S.L., Biron, P.M., Zimmermann, A., Venter, O., and Grant, J.W.A., 2010, Do in-stream restoration structures enhance salmonid abundance? A meta-analysis: Canadian Journal of Fisheries and Aquatic Sciences, v. 67, p. 831–841, doi: 10.1139/f10-021.

Yakima Basin Integrated Plan, 2023, https://yakimabasinintegratedplan.org/ (accessed March 2023).

Zotarelli, L., Dukes, M.D., Romero, C.C., Migliaccio, K.W., and Morgan, K.T., 2009, Step by step calculation of the penman-monteith evapotranspiration (FAO-56 Method), https://www.agraria.unirc.it/documentazione/materiale_didattico/1462_2016_412_24509.pdf (accessed June 2023).

APPENDICES

Appendix A – Input Parameters: Daily Totals and Averages

Date	Rn (MJ/m2/day)	Gmeadow (MJ/m2/day)	Griparian (MJ/m2/day)	Delta (kPa/C)	Tmean (C)	u2 (m/s)	RH (%)	es (kPa)	ea (kPa)
5/22/2023	7	1.85	-1.71	19.33	11.34	8.14	58.94	1.89	1.12
5/23/2023	7	3.23	1.23	20.08	11.95	4.92	57.53	2.23	1.28
5/24/2023	8	4.54	4.96	23.74	14.66	4.40	54.72	2.63	1.44
5/25/2023	8	4.25	5.21	25.14	15.60	2.89	61.02	2.59	1.58
5/26/2023	8	5.59	7.44	26.45	16.44	2.85	64.12	2.87	1.84
5/27/2023	8	3.81	4.78	30.35	18.75	4.78	51.45	3.20	1.65
5/28/2023	8	5.58	6.06	29.23	18.11	6.59	50.53	3.18	1.60
5/29/2023	8	5.15	5.34	29.41	18.22	7.42	46.80	3.24	1.51
5/30/2023	8	3.77	2.33	24.76	15.35	8.50	45.42	2.58	1.17
5/31/2023	7	2.79	-0.41	20.92	12.61	9.49	45.02	2.15	0.97
6/1/2023	9	4.47	4.67	23.07	14.19	5.09	43.93	2.63	1.15
6/2/2023	9	5.03	6.86	27.17	16.89	5.00	46.16	3.08	1.42
6/3/2023	9	5.49	7.80	30.31	18.73	5.04	37.97	3.54	1.34
6/4/2023	9	4.28	5.69	28.22	17.52	7.89	40.68	3.06	1.25
6/5/2023	10	4.48	6.29	30.82	19.01	7.34	31.85	3.53	1.13
6/6/2023	10	4.91	7.64	32.12	19.71	2.87	38.71	3.80	1.47
6/7/2023	11	5.20	8.89	36.19	21.76	3.25	37.81	4.34	1.64
6/8/2023	11	-4.67	7.88	38.31	22.75	5.20	40.80	4.26	1.74
6/9/2023	5	-1.47	-1.29	23.23	14.31	6.02	79.09	2.45	1.94
6/10/2023	9	-0.59	0.51	22.61	13.86	6.36	71.87	2.28	1.64
6/11/2023	10	6.16	8.69	29.82	18.45	4.42	60.31	3.52	2.12
6/12/2023	12	8.01	11.65	38.18	22.69	4.78	54.01	4.28	2.31

Date	Rn (MJ/m2/day)	Gmeadow (MJ/m2/day)	Griparian (MJ/m2/day)	Delta (kPa/C)	Tmean (C)	u2 (m/s)	RH (%)	es (kPa)	ea (kPa)
6/13/2023	10	2.31	2.61	30.81	19.00	8.32	52.54	3.19	1.68
6/14/2023	8	1.92	-0.48	20.88	12.58	9.12	53.63	2.07	1.11
6/15/2023	9	4.07	5.18	26.09	16.21	6.40	47.96	2.91	1.39
6/16/2023	9	5.07	6.93	30.15	18.64	6.66	51.97	3.31	1.72
6/17/2023	10	2.78	2.42	23.35	14.38	7.26	56.04	2.27	1.27
6/18/2023	10	2.14	-0.09	18.11	10.30	7.99	55.46	1.84	1.02
6/19/2023	10	1.86	0.35	18.11	10.31	7.72	56.99	1.80	1.02
6/20/2023	11.94	0.73	1.60	19.22	11.24	5.76	63.73	1.90	1.21
6/21/2023	11.00	4.01	4.78	24.64	15.27	3.59	55.81	2.55	1.42
6/22/2023	10.00	3.40	3.81	26.18	16.27	3.23	58.23	2.86	1.66
6/23/2023	10.36	1.44	3.19	27.57	17.13	3.65	56.24	3.14	1.76
6/24/2023	15.92	3.85	5.90	31.58	19.42	4.47	47.89	3.30	1.58
6/25/2023	16.27	4.69	7.01	32.49	19.91	4.47	47.29	3.57	1.69
6/26/2023	12.99	1.75	3.62	33.72	20.54	4.93	52.79	3.60	1.90
6/27/2023	17.82	5.79	7.76	34.16	20.76	5.23	55.25	3.89	2.15
6/28/2023	16.56	5.97	7.11	36.62	21.97	4.03	53.94	4.11	2.22
6/29/2023	17.00	5.79	7.70	39.26	23.18	5.51	46.44	4.25	1.98
6/30/2023	19.20	5.80	7.35	38.82	22.98	6.73	44.06	4.34	1.91
7/1/2023	18.94	4.16	5.21	33.72	20.54	7.07	44.24	3.48	1.54
7/2/2023	18.65	4.75	5.32	33.90	20.63	4.58	35.57	3.76	1.34
7/3/2023	18.53	4.42	4.46	34.45	20.91	3.21	32.57	3.76	1.22
7/4/2023	17.33	4.37	5.00	36.61	21.96	2.97	39.37	4.08	1.61
7/5/2023	15.25	4.01	4.97	38.25	22.72	2.74	42.14	4.16	1.75
7/6/2023	14.50	3.99	5.55	41.49	24.16	2.88	41.93	4.59	1.93

Appendix B – Output Evaporation and ET Rates

Date	Etdry (mm/day)	Etwet (mm/day)	Pan Evap (mm/day)	Kp	Corrected Evap (mm/day)	OpenET (mm/day)
5/22/2023	1.70	0.90		0.54		4.19
5/23/2023	1.74	0.78		0.63		4.55
5/24/2023	1.83	0.69		0.64		4.30
5/25/2023	1.64	0.63		0.70		4.03
5/26/2023	1.56	0.54	3.32	0.71	2.34	4.20
5/27/2023	1.94	0.61	3.79	0.62	2.35	4.74
5/28/2023	1.98	0.62	4.07	0.57	2.30	5.19
5/29/2023	2.14	0.66	4.47	0.53	2.38	5.85
5/30/2023	2.20	0.85	3.95	0.50	1.96	5.03
5/31/2023	2.22	1.03	3.74	0.47	1.75	4.32
6/1/2023	2.28	0.87	2.65	0.59	1.56	4.66
6/2/2023	2.17	0.70	3.22	0.60	1.93	4.81
6/3/2023	2.63	0.74	3.05	0.57	1.74	5.03
6/4/2023	2.46	0.80	4.64	0.50	2.31	5.22
6/5/2023	3.14	0.89	4.04	0.48	1.94	5.66
6/6/2023	2.58	0.68	3.17	0.64	2.01	6.64
6/7/2023	2.64	0.61	2.93	0.62	1.82	6.34
6/8/2023	2.45	0.58	2.23	0.58	1.29	5.34
6/9/2023	1.26	0.52	0.83	0.65	0.54	1.94
6/10/2023	1.39	0.61	1.55	0.62	0.97	2.22
6/11/2023	1.66	0.47	1.26	0.65	0.82	5.85
6/12/2023	1.85	0.43	2.80	0.63	1.75	6.74

Date	Etdry (mm/day)	Etwet (mm/day)	Pan Evap (mm/day)	Kp	Corrected Evap (mm/day)	OpenET (mm/day)
6/13/2023	1.90	0.60		0.52		6.00
6/14/2023	1.86	0.90	1.80	0.50	0.90	5.46
6/15/2023	2.09	0.72	3.08	0.56	1.74	6.38
6/16/2023	1.92	0.58	2.95	0.57	1.68	5.90
6/17/2023	1.78	0.79	4.09	0.56	2.30	5.19
6/18/2023	1.80	0.98	2.60	0.54	1.40	4.52
6/19/2023	1.75	0.98	2.59	0.55	1.42	3.99
6/20/2023	1.57	0.83	1.98	0.62	1.23	3.52
6/21/2023	1.79	0.70	1.71	0.67	1.14	5.49
6/22/2023	1.72	0.60	2.38	0.68	1.62	5.51
6/23/2023	1.78	0.57	1.83	0.67	1.21	6.28
6/24/2023	2.09	0.63	2.34	0.62	1.45	6.29
6/25/2023	2.11	0.59	2.83	0.62	1.75	6.78
6/26/2023	1.89	0.53	1.75	0.62	1.08	5.76
6/27/2023	1.81	0.47	2.31	0.62	1.43	5.20
6/28/2023	1.85	0.45	2.31	0.65	1.50	5.20
6/29/2023	2.15	0.51	3.34	0.59	1.95	6.01
6/30/2023	2.27	0.52	4.63	0.54	2.52	6.57
7/1/2023	2.26	0.65	4.67	0.53	2.49	6.32
7/2/2023	2.81	0.75	3.86	0.57	2.22	5.94
7/3/2023	3.07	0.82	2.96	0.60	1.78	5.99
7/4/2023	2.54	0.62	2.44	0.63	1.55	4.85
7/5/2023	2.37	0.57	2.51	0.65	1.64	4.80
7/6/2023	2.38	0.52	2.18	0.65	1.41	5.38

Appendix C – Composite Aerial Imagery

May 2nd, 2023:

May 26th, 2023:

June 7th, 2023:

June 29th, 2023: